GEORGIA INSTITUTE OF TECHNOLOGY
OFFICE OF CONTRACT ADMINISTRATION
SPONSORED PROJECT INITIATION

Date: 2/10/79

Project Title: Global Atmospheric Measurements Experiment on Tropospheric Aerosols and Gases (GAMETAG)

Project No: G-35-650

Project Director: Dr. Douglas D. Davis

Sponsor: National Science Foundation, Washington, D. C. 20550

Agreement Period: From 2/15/78 Until 5/31/80*

*Includes 6 month flexibility period

Type Agreement: Grant No. ATM-7823598 (thru G.I.T.)

Amount: $285,700 NSF Funds (G-35-650)
14,000 GIT Contribution (G-35-337)
$299,700 TOTAL

Reports Required: Annual Progress Reports; Final Project Report

Sponsor Contact Person (s):

Technical Matters

Dr. Robert J. McNeal
Division of Atmospheric Sciences
National Science Foundation
1800 G. Street, N.W.
Washington, D.C. 20550

Phone: (202)632-1976

Contractual Matters
(thru OCA)

Ms. Lois A. Shapiro
Grants Specialist - Area 4
National Science Foundation
1800 G. Street, N.W.
Washington, D.C. 20550

Phone: (202) 632-5884

NOTE: FOLLOW-ON PROJECT TO G-35-632.

Defense Priority Rating: N/A

Assigned to: Geophysical Sciences (School/Laboratory)

COPIES TO:

Project Director
Division Chief (EES)
School/Laboratory Director
Dean/Director–EES
Accounting Office
Procurement Office
Security Coordinator (OCA)
Reports Coordinator (OCA)

Library, Technical Reports Section
EES Information Office
EES Reports & Procedures
Project File (OCA)
Project Code (GTRI)
Other

CA–3 (3/76)

GEORGIA INSTITUTE OF TECHNOLOGY OFFICE OF CONTRACT ADMINISTRATION

SRH48

SPONSORED PROJECT TERMINATION SHEET

Date 9/8/82

Project Title: Global Atmospheric Measurements Experiment on Tropospheric Aerosols and Gases (GAMETAG)

Project No: G-35-650

Project Director: Dr. Douglas D. Davis

Sponsor: National Science Foundation

Effective Termination Date: 11/30/80

Clearance of Accounting Charges: _____

Grant/Contract Closeout Actions Remaining:

- [x] Final Invoice and Closing Documents
- [ ] Final Fiscal Report
- [x] Final Report of Inventions (positive only)
- [x] Govt. Property Inventory & Related Certificate
- [ ] Classified Material Certificate
- [ ] Other _____

Assigned to: GEO SCI (School/~~laboratory~~)

COPIES TO:

~~Administrative Coordinator~~ RAN
Research Property Management / Accounting
Procurement/EES Supply Services
Research Security Services
Reports Coordinator (OCA)
Legal Services (OCA)
Library
EES Public Relations (2)
~~Computer Input~~
Project File
Other OTRI

FORM OCA 10:781

G 35-650

NATIONAL SCIENCE FOUNDATION
Washington, D.C. 20550

FINAL PROJECT REPORT
NSF FORM 98A

PLEASE READ INSTRUCTIONS ON REVERSE BEFORE COMPLETING

PART I–PROJECT IDENTIFICATION INFORMATION

1. Institution and Address	2. NSF Program	3. NSF Award Number
Georgia Institute of Technology School of Geophysical Sciences Atlanta, GA 30332	Atmospheric Sciences	ATM-7823598
	4. Award Period From 1/79 To 11/80	5. Cumulative Award Amount $304,437

6. Project Title
Global Atmospheric Measurement Experiment on Tropospheric Aerosols and Gases (GAMETAG)

PART II–SUMMARY OF COMPLETED PROJECT *(FOR PUBLIC USE)*

The third year renewal of the Phase I GAMETAG project had as its major goal the completion of all data analysis, the publication of results, and the data achieving of the 1978 GAMETAG flight data. Secondary goals were: (1) the making of further improvements in the LIF OH system; and (2) the formulation of a Phase II GAMETAG program.

Concerning the major objective, virtually all aspects of this objective have been completed. It should be noted, however, that manuscripts are still, and undoubtedly will continue to be written on GAMETAG data (see attachment B). All 1978 GAMETAG flight data is now available (on magnetic tape) to any investigator wishing to use the data. These data are organized according to flight date and flight hour such that all chemical and physical variables measured can be acquisitioned at the same time for any given flight interval (see attachment A).

The number of publications by GAMETAG principal investigators is now 20 (17 of which are already in print) and there are at least an equal number of papers by other authors who have cited GAMETAG results.

Concerning the planning of a GAMETAG Phase II program, as can be seen from attachment C, a draft of a Phase II program was completed by the GAMETAG executive committee.

Regarding our laser improvement program, the principal focus of this effort has been on quantifying the magnitude of the $O_3/H_2O/OH$ interference problem (see attachments D, E, and F) in the detection of OH by the SP-LIF technique. The latter study has been followed by a redesigning effort in which extremely short laser pulses (i.e., $\leq$ 1 ns) have been used to overcome the laser-induced OH formation problem.

PART III–TECHNICAL INFORMATION *(FOR PROGRAM MANAGEMENT USES)*

1. ITEM *(Check appropriate blocks)*	NONE	ATTACHED	PREVIOUSLY FURNISHED	TO BE FURNISHED SEPARATELY TO PROGRAM	
				Check (✓)	Approx. Date
a. Abstracts of Theses			✓		
b. Publication Citations		✓			
c. Data on Scientific Collaborators			✓		
d. Information on Inventions	✓				
e. Technical Description of Project and Results		✓			
f. Other *(specify)*					

2. Principal Investigator/Project Director Name *(Typed)*	3. Principal Investigator/Project Director Signature	4. Date
		8/25/82

NSF Form 98A (5/78) Supersedes All Previous Editions

Form Approved OMB No. 99R0013

Attachment "A"

JOURNAL OF GEOPHYSICAL RESEARCH, VOL. 85, NO. C12, PAGES 7285–7292, DECEMBER 20, 1980

Project Gametag: An Overview

D. D. DAVIS

School of Geophysical Sciences, Georgia Institute of Technology, Atlanta, Georgia 30332

Presented in this first paper of the Gametag series is an overview of the Gametag program. This presentation is intended to provide the reader with background information about several of the important characteristics of the program. These include (1) the sampling strategy and general philosophy of the program; (2) the field-sampling track; (3) the nature of the sampling platform; (4) a listing of instruments and measurements recorded; (5) Gametag data-archiving procedures; and (6) a listing of participating institutions, scientific team members, and principal investigators.

INTRODUCTION

In this issue of the *Journal of Geophysical Research,* 12 papers are presented that reflect some of the important findings from the 2-year field-sampling program known by the acronym Gametag (Global Atmospheric Measurements Experiment on Tropospheric Aerosols and Gases). Several other Gametag papers have already been published before this issue [*Huebert and Lazrus,* 1978; *Danielsen,* 1980; *Danielsen and Hipskind,* 1980; *Schiff et al.,* 1979], and it is expected that several additional papers will follow in the coming months. In the text below, the author has attempted to describe the important characteristics of the Gametag program and thus render the sequence of papers that follows more meaningful.

SAMPLING STRATEGY AND GENERAL PHILOSOPHY OF PROGRAM

It is now generally recognized that the trace gas and aerosol species which collectively define the chemistry of the troposphere are coupled together with time constants ranging from seconds to years. Representative of those species involved in fast chemical coupling are the various nitrogen and oxygen species shown in Figures 1 and 2. These figures illustrate the importance of making simultaneous measurements of species during field sampling. This mode of sampling becomes of critical importance in the testing of chemical models that are designed to predict concentrations of short-lived photochemical species. For species having lifetimes of a few days or longer the impact of atmospheric transport must also be seriously considered. In this case simultaneous measurements can prove to be quite valuable but not necessarily definitive in model testing.

The Gametag program was designed to provide a limited but meaningful test of present models for short-lived photochemical species and also to provide survey data on these and numerous other longer-lived species over an extensive latitude range. Both before and during this field measurement program, numerous scientific questions have been raised, some of which follow: What is the relative importance of photochemical and transport processes in controlling the global distribution of O_3? What is the impact of pollution versus natural sources in dictating the tropospheric distribution of CO? What is the global distribution of methyl chloroform, and can this be systematically related to the global OH distribution? What evidence exists for gas to aerosol conversion in the clean troposphere? What is the relative importance of natural versus pollution sources in controlling global SO_2 levels? What is the role of the oceans in controlling boundary layer trace gas concentrations? What is the global distribution of NO_x species?

The above listing is not intended to imply that all or even most of these questions originated with the conception and deployment of Gametag; rather, it is an indication of the types of questions to which Gametag data are now believed to be directly applicable.

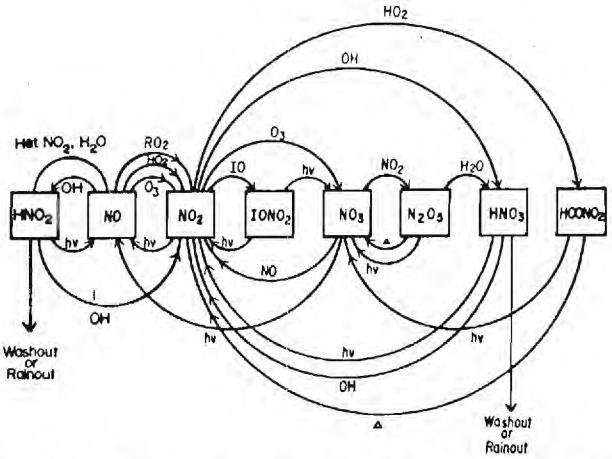

Fig. 1. A possible daytime tropospheric chemical scheme involving nitrogen oxide species (modified from *Levy* [1974]).

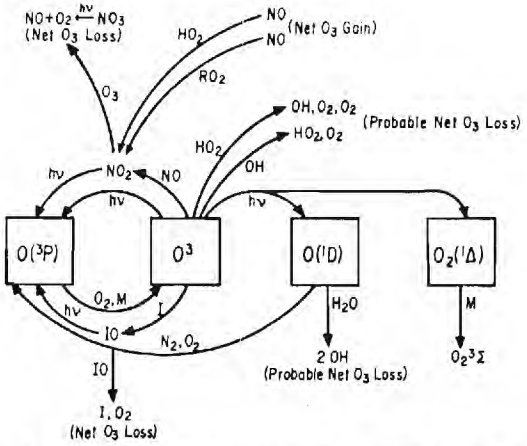

Fig. 2. A possible daytime tropospheric chemical scheme showing the key reactions of active oxygen (modified from *Levy* [1974]).

Paper number 80C0757.
0148-0227/80/080C-0757$01.00

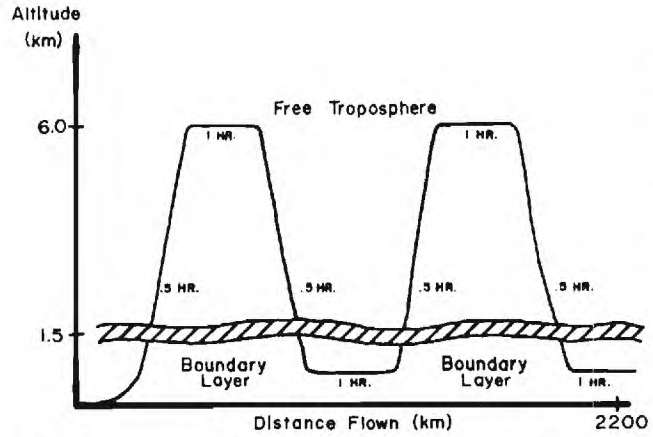

Fig. 3. Blueprint aircraft flight pattern used during the 1977 and 1978 Gametag flight operations.

In addition to 'simultaneous measurements' being a fundamental part of the sampling strategy in Project Gametag a second important aspect of the field-sampling scenario was that of making measurements both in and above the atmospheric boundary layer. The latter sampling approach was dictated by the fact that tropospheric trace gases can have both biospheric and atmospheric sources and sinks. Thus by measuring the concentration gradients of species between the boundary layer and the free troposphere it was believed that considerable insight could be gained into the relative importance of these different sink/source regimes. Based on this strategy, the 'blueprint' sampling profile that was to be flown during Gametag flights is that of Figure 3. Since the typical flight was limited to approximately 6½ hours, the profile in Figure 3 suggests that there normally would be two 1-hour boundary layer and two 1-hour free tropospheric flight legs during each flight operation. In operating between 1 and 6 km the two ascents and descents would also each take ~0.5 hour. In actual fact, it was rarely possible to execute the blueprint sampling profile given in Figure 3 for two reasons: First, the sampling strategy of covering a large latitude range, using a single aircraft, required that virtually every flight involve moving to a new geographical location some 1200–2000 miles away. Each move to a new location, however, was controlled by a 2- to 3-day logistics period, a period that frequently was not synchronized with the presence of good weather conditions between the point of initiation and the final destination. The second problem area, as will be discussed later in the pa-

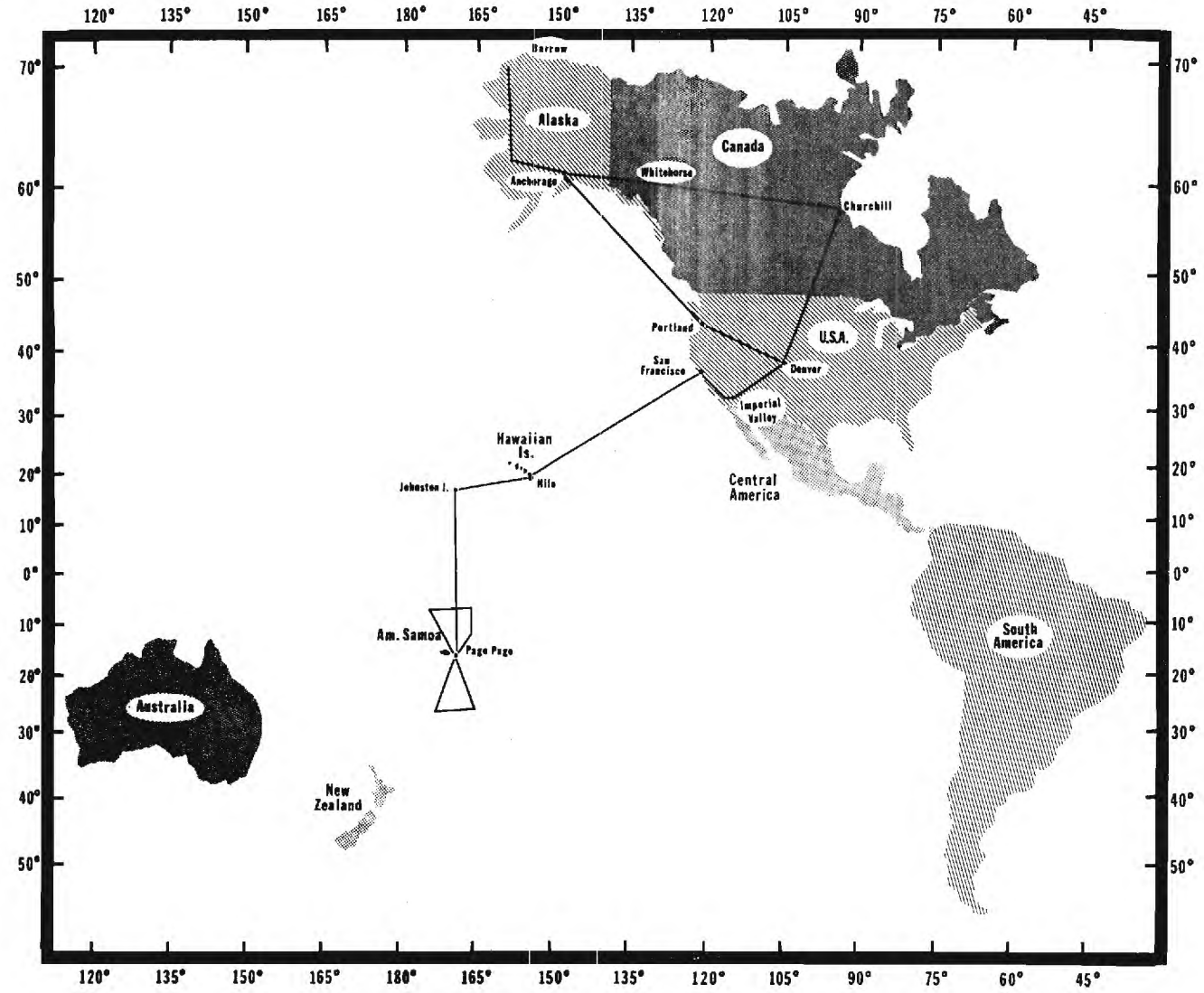

Fig. 4. Flight track of the 1977 Gametag field-sampling program.

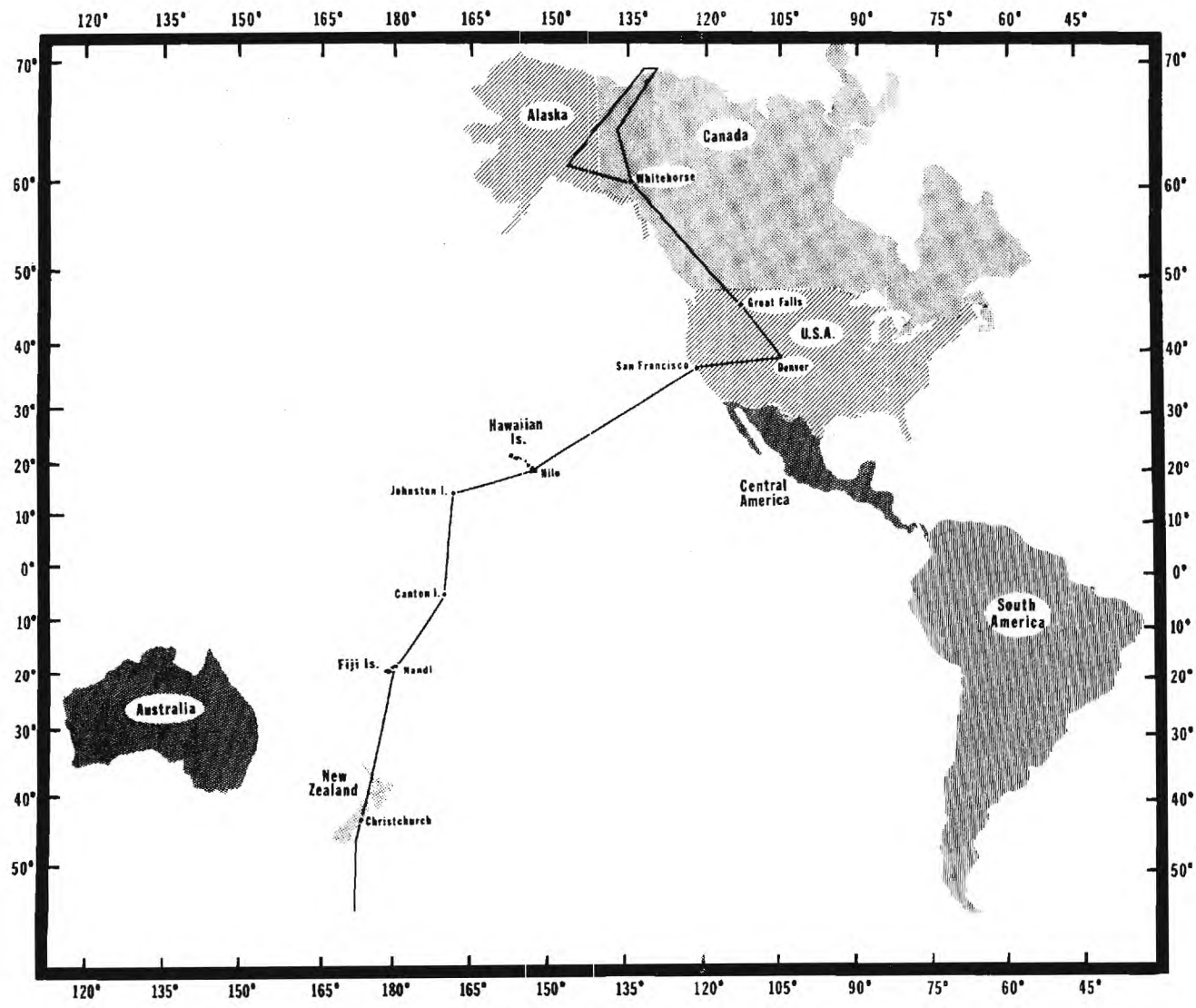

Fig. 5. Flight track of the 1978 Gametag field-sampling program.

per, involved the fact that flight profiles in the Pacific had to be tuned to take into account the low density of landing sites equipped to handle large aircraft. Flying extra long distances, for example, required stretching aircraft fuel, which, in turn, meant flying at high altitudes where engine efficiency was higher. Thus high-altitude flying dictated by condition 2 together with the high-altitude flying requirements to avoid harsh weather as defined by condition 1 resulted in nearly 3 times more flight hours logged in the free troposphere than in the boundary layer. Even so, it will be seen that the limited boundary layer sampling did produce some very significant results.

FIELD-SAMPLING TRACK

It should be noted that the word 'global' in the title of the Gametag program is being used here in a limited context. Actual sampling of the entire global troposphere was not achieved in the 2 years of field operations of Project Gametag; instead, a 'select' global sampling strategy was carried out. The major emphasis of this program was placed on covering the maximum possible latitude range in both the northern and the southern hemisphere (see Figures 4 and 5) and of carrying out sampling over both ocean and land areas. A detailed listing of the exact date and location of each flight during the 1977 and 1978 field experiments has been provided in Table 1. It will be noticed from Figures 4 and 5 that the northward and southward flight tracks in the South Pacific operation and in the Canadian-Alaska flights were in most cases largely redundant. In these instances, data were obtained from the same geographical area over time periods ranging from 2 days up to 2 weeks. Thus one might characterize this type of data collection as a 'long time exposure' rather than a quick 'snapshot' of the atmosphere. The effects of this extended sampling time are most clearly seen in the ozone and H_2O data for the northward and southward flight tracks in the South Pacific [see *Routhier et al.*, this issue; *Routhier and Davis,* this issue].

The selection of the Pacific Ocean and Canada/Alaska as the major regions over which sampling was carried out was dictated by a combination of factors, some of which were scientific, others logistical. In the case of Canada and the many islands in the Pacific Ocean, diplomatic permission for overflying and/or landing in their territories was relatively easy to

TABLE 1. Detailed Flight Track During the 1977 and 1978 Gametag Field Program

Date	Initiation	Destination	Significant Turning Points
		1977	
Aug. 7	Denver 39.6°N, 104.5°W	Portland 46.8°N, 122.7°W	
Aug. 8	Portland 46.8°N, 122.7°W	Anchorage 61.2°N, 150°W	50°N, 144.6°W
Aug. 9	Anchorage 61.2°N, 150°W	Anchorage 61.2°N, 150°W	64°N, 157.5°W 70.7°N, 159°W
Aug. 11	Anchorage 61.2°N, 150°W	Churchill 58.8°N, 94.2°W	stop at Whitehorse 60.2°N, 134.8°W
Aug. 12	Churchill 58.8°N, 94.2°W	Denver 39.6°N, 104.5°W	
Aug. 22	Denver 39.6°N, 104.5°W	San Francisco 37.5°N, 122.1°W	33°N, 115°W
Aug. 23	San Francisco 37.5°N, 122.1°W	Hilo, Hawaii 20°N, 155°W	
Aug. 25	Hilo, Hawaii 20°N, 155°W	Johnston Island 16.8°N, 169.5°W	19.5°N, 169.5°W
Aug. 26	Johnston Island 16.8°N, 169.5°W	Pago Pago 14.3°N, 170.8°W	
Aug. 28	Pago Pago 14.3°N, 170.8°W	Pago Pago 14.3°N, 170.8°W	8°S, 171°W 8°S, 168°W
Aug. 31	Pago Pago 14.3°N, 170.8°W	Pago Pago 14.3°N, 170.8°W	25.5°S, 170°W 25.5°S, 174°W
Sept. 1	Pago Pago 14.3°N, 170.8°W	Johnston Island 16.8°N, 169.5°W	
Sept. 2	Johnston Island 16.8°N, 169.5°W	Hilo, Hawaii 20°N, 155°W	13.0°N, 160.5°W
Sept. 5	Hilo, Hawaii 20°N, 155°W	San Francisco 37.5°N, 122.1°W	
Sept. 6	San Francisco 37.5°N, 122.1°W	Denver 39.6°N, 104.5°W	33°N, 155°W
		1978	
April 27	Denver 39.6°N, 104.5°W	San Francisco 37.5°N, 122.1°W	33°N, 115°W
April 28	San Francisco 37.5°N, 122.1°W	Hilo, Hawaii 20°N, 155°W	
May 2	Hilo, Hawaii 20°N, 155°W	Johnston Island 16.8°N, 169.5°W	
May 3	Johnston Island 16.8°N, 169.5°W	Canton Island 2.5°S, 171.1°W	
May 4	Canton Island 2.5°S, 171.1°W	Fiji Islands 17.7°S, 177.4°E	
May 6	Fiji Islands 17.7°S, 177.4°E	Christchurch, N.Z. 43.8°S, 172.6°E	
May 10	Christchurch, N.Z. 43.8°S, 172.6°E	Christchurch, N.Z 43.8°S, 172.6°E	58°S, 172.0°E
May 11	Christchurch, N.Z. 43.8°S, 172.6°E	Fiji Islands 17.7°S, 177.4°E	
May 12	Fiji Islands 17.7°S, 177.4°E	Canton Island 2.5°S, 171.1°W	
May 13	Canton Island 2.5°S, 171.1°W	Johnston Island 16.8°N, 169.5°W	
May 14	Johnston Island 16.8°N, 169.5°W	Hilo, Hawaii 20°N, 155°W	
May 17	Hilo, Hawaii 20°N, 155°W	San Francisco 37.5°N, 122.1°W	
May 18	San Francisco 37.5°N, 122.1°W	Denver 39.6°N, 104.5°W	33°N, 115°W
May 27	Denver 39.6°N, 104.5°W	Great Falls 47.0°N, 113.0°W	
May 28	Great Falls 47.0°N, 113.0°W	Whitehorse 60.2°N, 134.8°W	
May 30	Whitehorse 60.2°N, 134.8°W	Whitehorse 60.2°N, 134.8°W	62.9°N, 144.5°W 70.0°N, 132.5°W
May 31	Whitehorse 60.2°N, 134.8°W	Great Falls 47.0°N, 113.0°W	
June 1	Great Falls 47.0°N, 113.0°W	Denver 39.6°N, 104.5°W	

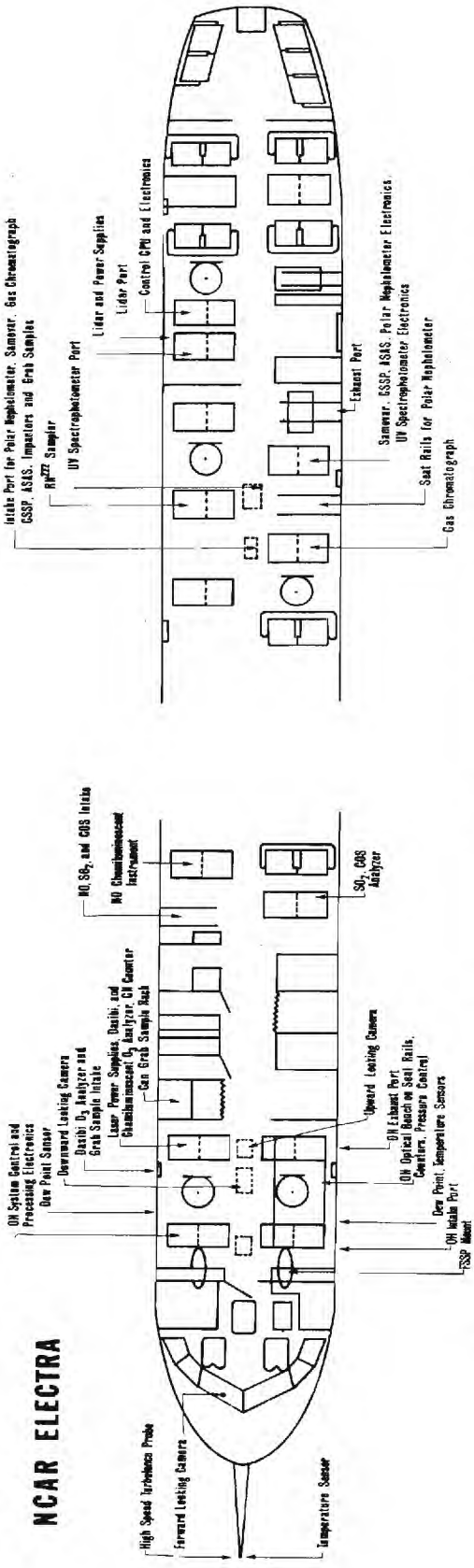

Fig. 6. Gametag instrumentation layout aboard the NCAR L-188C Electra (the forward section of the aircraft is shown on the left).

obtain. For many other areas also of great scientific interest to us, 1–2 years would have been required to obtain the same diplomatic clearance.

A major consideration in defining the detailed flight track over the Pacific Ocean was the rather limited range of the aircraft versus the density of islands with large enough runways to handle four-engine aircraft, appropriate aircraft fuel, and food and lodging facilities for the crew and scientific team members.

SAMPLING PLATFORM

The sampling platform used throughout the Gametag program was the L-188C turboprop Electra owned and operated by the National Center for Atmospheric Research (NCAR). This aircraft, when fully outfitted with Gametag instrumentation plus spare parts and personal baggage, had a nominal operating ceiling of 6.4 km and a range, at that altitude, of ~3200 km. For the flights between the U.S. mainland and Hawaii the weight of the aircraft was further reduced, thereby increasing the range by ~500 km. In the latter case, all spare parts and several flight crew and scientific personnel were shipped to the next stopping point via commercial jets. As was noted earlier, when following the blueprint Gametag sampling scenario, involving both boundary layer and free tropospheric sampling, the effective range of the Electra was reduced to ~2200 km.

The field operations team consisted of six to seven aircraft personnel (pilot, copilot, flight engineer, aircraft mechanic, and two or more electronic computer technicians) and 13–14 scientific crew members.

The instrumentation aboard the Electra consisted of instruments operated by both university and NCAR scientists as well as those maintained by NCAR aircraft personnel. Instruments in the latter category were primarily meteorological sensors such as those used to measure temperature, dew point, and horizontal and vertical winds. In addition to maintaining the meteorological sensors, NCAR flight technicians also maintained a Nova 1200 computer system. This data management system was used to store position and time information, all meteorological data, and real-time data from several instruments collecting chemical information.

The location of each instrument on the Electra aircraft is shown in Figure 6. Although some of the chemical sensors were relatively insensitive to location, others were not. In the case of the OH detector a primary concern was the need to sample air well outside the aircraft skin boundary layer. To ensure that this was the case and that relatively nonturbulent air entered the air scoop, the OH detection system was placed in the forward cabin of the aircraft. The exhaust port for this instrument was approximately 4 in. in diameter and was located on the port side of the Electra. To minimize any possible contamination from the exhaust of this system, all other chemical sensors had their intake ports either on the top center line of the aircraft or on the starboard side. In a further effort to minimize the possibility that the exhaust from one instrument might contaminate the intake of a second instrument behind it, the exhausts from all other real-time sampling instruments were dumped into a common large-diameter 'garbage' line. This garbage line exhausted near the rear of the aircraft on the port side. A final consideration on the location of several instruments was that of contamination from the aircraft engines. Tests were performed a year before the first

TABLE 2. Gametag Measurements

Variable Measured	Technique	Time Resolution	Principal Investigator
O_3	UV absorption	10 s	D. D. Davis and T. Delany
	chemiluminescence	3–4 s	
OH	laser-induced fluorescence	3–15 min	D. D. Davis
H_2O	two-stage thermoelectric hygrometer	2–3 s	NCAR RAF and D. D. Davis
UV flux	ultraviolet spectroirradiometer	2 min	B. Sellers
NO	chemiluminescence	1–2 min	H. Schiff
HNO_3	filter matte collection—wet laboratory chemical analysis	45–60 min	B. Huebert and A. Lazrus
NO_3^-	filter matte collection—wet laboratory chemical analysis	45–60 min	B. Huebert and A Lazrus
SO_4^{-2}			
Cl^-			
NH_4^+			
^{222}Rn	filter matte collection with on-board β counting	20–60 min	B. Huebert
SO_2	cryo trapping with on-board GLC flame photometric analysis	4–7 min	A. Bandy
COS			
N_2O	air stream aliquot sampling with on-board GC flame ionization and/or electron capture analysis	5–15 min	L. Heidt
CO			
CH_3CCl_3			
CCl_4			
F-11			
F-12			
CO	grab sampling laboratory GC or GLC/flame ionization and/or electron capture analysis	not relevant	L. Heidt R. Rasmussen
N_2O			
CCl_4			
CH_3CCl_3			
F-11			
F-12			
CH_4			
CO_2	grab sampling laboratory GC or GLC/flame ionization and/or electron capture analysis	not relevant	R. Rasmussen
CH_3Cl			
C_2H_2			
C_2H_4			
C_2H_6			
Intermediate molecular weight hydrocarbons			
Intermediate molecular weight hydrocarbons	absorption on Tenax, GC/mass spectrometer analysis	not relevant	R. Seivers and T. Delany
Aerosol optical properties	polar nephelometer	10–15 min	G. Grams and E. Patterson
Aerosol size/number distributon	Knollenberg spectrometers	2 s	T. Delany and E. Patterson
Dew Point	two-stage thermoelectric hygrometer	2–3 s	NCAR RAF and D. D. Davis
Air temperature	platinum resistance thermometer		NCAR RAF
IR ground emissions	bolometric radiometer		NCAR RAF
Broadband upward and downward UV flux	broadband pyranometer	1–2 s	NCAR RAF and B. Sellers
True air speed	aircraft computed		
Horizontal winds	aircraft computed		
Vertical gust velocities	aircraft computed		
Geographical Position	aircraft computed		
Potential temperature	aircraft computed		
Vertical acceleration	aircraft computed		

NCAR RAF is the National Center for Atmosphere Research, Research Aviation Facility.

Gametag flights to determine the magnitude of this problem. In these tests, CO samples were collected from several locations along the port side of the Electra, some being in front of the prop line, others even with the prop line, and still several others at different positions behind the prop line. The results from these experiments indicated that the CO levels at the several different positions agreed with each other to within the experimental random error (±3%) for the measurements. Even so, it was recognized that some measurements (i.e., NO) could be influenced very significantly by even low levels of contamination, and thus the intakes for these systems were either even with the prop line, in front of it, or located overhead on the aircraft center line. To minimize contamination of the intakes while the aircraft was on the ground, all intake ports were routinely capped off upon landing.

MEASUREMENTS

Table 2 lists the variables that were measured during the Gametag field operation. Also listed in this table are the technique(s) that were employed in measuring a specific variable together with the time resolution of the instrument and the principal investigator(s) (PI) with major responsibility for the equipment and/or analyzing the data.

It will be noticed that the time resolution for the Gametag instrument array varied from a relatively short response time of 1 s to a very low resolution sampling time of ~60 min. Most of the real-time measurements, however, had a time resolution of 15 min or shorter and thus provided a reasonable basis for the testing of photochemical models. In the case of the grab samples, which were collected in the field and later ana-

TABLE 3. Participating Institutions

Institution	Scientific Team Members	Principal Investigator
Colorado College	B. J. Huebert	B. J. Huebert
Drexel University	A. R. Bandy	A. R. Bandy
	P. J. Maroulis	
	A. L. Torres	
	A. B. Goldberg	
Georgia Institute of Technology	D. D. Davis	D. D. Davis
	D. Philen	
	W. Heaps	
	M. Rodgers	
	R. Dennett	
	D. Putman	
	F. Routhier	
Georgia Institute of Technology	G. W. Grams	G. W. Grams and E. Patterson
	E. Patterson	
	C. Wyman	
	C. S. Kiang	
National Center for Atmospheric Research	L. Heidt	L. Heidt
	J. Krasnec	
	W. H. Pollock	
National Center for Atmospheric Research	T. Delany	T. Delany
	A. Wartburg	
National Center for Atmospheric Research	A. L. Lazrus	A. L. Lazrus
National Center for Atmospheric Research	P. Haagenson	flight meteorologist
Oregon State University	E. Danielsen	E. Danielsen
	R. S. Hipskind	
Oregon Graduate Center	R. A. Rasmussen	R. A. Rasmussen
	L. E. Rasmussen	
	M. A. K. Khalil	
	R. W. Dalluge	
Panametrics	B. Sellers	B. Sellers
	F. A. Hanser	
	J. Hunerwadel	
York University	H. Schiff	H. Schiff
	D. Pepper	
	B. Ridley	
University of Colorado	R. Sievers	R. Sievers
	D. W. Denney	
	R. M. Barkley	
Florida State University	A. C. D. Leslie	A. C. D. Leslie

lyzed in the laboratory, the results must be viewed in terms of a set of unconnected snapshots of the atmosphere.

A final point concerning Table 2 is that not in all cases were quantitative data collected for all variables in both 1977 and 1978. The 1977 flights, in particular, resulted in the identification of calibration problems in several instruments, problems which had not appeared in any of the advance test flights. The respective PI's for these instruments have therefore looked upon their 1977 data as being qualitative in nature.

In contrast to the 1977 flights, ~90% of all instrumentation aboard the Electra in 1978 produced quantitative data. For this reason the reader will generally see a heavier emphasis on 1978 results than on those from 1977. Also reflecting the larger abundance of quantitative data in 1978 has been the decision by the Gametag executive committee to archive the 1978 data first with a later follow-up on the smaller data base from 1977.

ARCHIVING OF DATA

One of the major considerations involved in defining the archiving scheme for Gametag data was selection of a format that would be relatively easy to use. Details on this procedure have been provided by R. Dennett et al. (unpublished manuscript, 1980). A brief summary of the latter document is provided below.

Because of the large amounts of data collected for several of the variables, magnetic tapes were chosen as the principal storage medium. Data are placed on these tapes in the form of card images, each card image representing one update interval. Although it is recognized that this is not the most concise form of storage, it is nevertheless a widely recognized form of information interchange. In an effort to reduce the amount of data that has to be stored on a data tape, only updates in the value of each variable are stored. This approach has greatly reduced the amount of computer memory required for data playback. The organizational scheme for archived Gametag data is as follows:

1. Each data tape contains data from a single flight day.
2. The first file on the tape contains information about the flight track and general comments regarding the data or the instruments used to record it.
3. Each of the remaining files on the tape represents 1 hour of data from a given flight day.
4. The first record within each of these data files initializes the data table in the computer memory. Each successive record then updates the values of all variables.

PARTICIPATION IN PROGRAM

Listed in Table 3 are the several organizations which played the major roles in defining the 1977/1978 Gametag program. In all, seven universities, one private research institute, the NSF-supported National Center for Atmospheric Research,

and one private company were actively involved. The scientific team members from each participating organization have been listed in Table 3 along with the senior scientist who served as principal investigator on each project. The executive committee during the program consisted of C. S. Kiang (Georgia Institute of Technology), R. Duce (University of Rhode Island), P. Crutzen (National Center for Atmospheric Research), and this author (Georgia Institute of Technology). Not listed are the names of the many people at the NCAR Research Aviation Facility who spent numerous hours working with the executive committee and individual Gametag scientists to help make this project a success. Most notable among these were the pilots, L. Newcomer, G. Summers, W. Zinser, and J. Covington; the flight engineer, J. Lundahl; the flight mechanic, H. Barber; the electronic and computer technicians, R. Taylor and M. Reynolds; and the interface/structural engineer, N. Zrubek.

The program is also greatly indebted to the members of the NCAR Aviation Panel, who provided for the necessary flight hours on the Electra, and to the National Science Foundation, which provided all the financial support for the project.

REFERENCES

Danielsen, E. F., Stratospheric source for unexpectedly large values of ozone measured over the Pacific Ocean during Gametag, August 1977, *J. Geophys. Res., 85,* 401–412, 1980.

Danielsen, E. F., and R. S. Hipskind, Stratospheric-tropospheric exchange at polar latitudes in summer, *J. Geophys. Res., 85,* 393–400, 1980.

Huebert, B., and A. Lazrus, Global tropospheric measurements of nitric acid vapor and particulate nitrate, *Geophys. Res. Lett., 5,* 577, 1978.

Levy, H., Tropospheric photochemistry, *Adv. Photochem., 9,* 369–523, 1974.

Routhier, F., and D. D. Davis, Free tropospheric and boundary layer airborne measurements of H_2O over the latitude range of 58°S to 70°N: Comparison with simultaneous high-resolution ozone measurements, *J. Geophys. Res.,* this issue.

Routhier, F., R. Dennett, P. Haagenson, and D. D. Davis, Free tropospheric and boundary layer airborne measurements of ozone over the latitude range of 58°S to 70°N, *J. Geophys. Res.,* this issue.

Schiff, H. I., D. Pepper, and B. A. Ridley, Tropospheric NO measurements up to 7 km, *J. Geophys. Res., 84,* 7895, 1979.

(Received January 28, 1980;
revised June 2, 1980;
accepted June 4, 1980.)

ATTACHMENT B GAMETAG Principal Investigators' Publications

"Global Tropospheric Measurements of Nitric Acid Vapor and Particulate Nitrate," Geo. Res. Lett., 5, 577, B. Huebert, and A. Lazrus [1980].

"Stratospheric Source for Unexpectedly Large Values of Ozone Measured Over the Pacific Ocean during GAMETAG, August 1977," Jrnl. Geo. Res., 85, 401, E.F. Danielsen [1980].

"Stratospheric-Tropospheric Exchange at Polar Latitudes in Summer," Jrnl. Geo. Res., 85, 393, E.F. Danielsen, and R.S. Hipskind [1980].

"Tropospheric NO Measurements up to 7 km," Jrnl. Geo. Res., 85, 7895, H.I. Schiff, D. Pepper, and B.A. Ridley, [1979].

"Project GAMETAG : An Overview," Jrnl. Geo. Res., 85, 7285, D.D. Davis [1980].

"Free Tropospheric/Boundary-Layer Airborne Measurements of H_2O Over the Latitude Range of 58°S to 70°N: Comparison with Simultaneous Ozone and Carbon Monoxide Measurements," Jrnl. Geo. Res., 85, 7293, F. Routhier and D.D. Davis [1980].

"Free Tropopsheric and Boundary-Layer Airborne Measurements of Ozone Over the Latitude Range of 58°N to 70°N," Jrnl. Geo. Res., 85, 7307, F. Routhier, R. Dennett, D.D. Davis, A. Wartburg, P. Haagenson, and A.C. Delany, [1980].

"Tropospheric Gas-Phase and Particulate Nitrate Measurements," Jrnl. Geo. Res., 85, 7322, B.J. Huebert, and A.L. Lazrus, [1980].

"Latitudinal Distributions of CO and CH_4 over the Pacific," Jrnl. Geo. Res., 85, 7329, L.E. Heidt, J.P. Krasnec, R.A. Lueb, W.H. Pollock, B.E. Henry, and P.J. Crutzen, [1980].

"Bulk Composition of Aerosols in the Remote Troposphere," Jrnl. Geo. Res., 85, 7337, B.J. Huebert, and A.L. Lazrus [1980].

"Atmospheric SO_2 Measurements on Project GAMETAG," Jrnl. Geo. Res., 85, 7345, P.J. Maroulis, A.L. Torres, A.B. Goldberg, and A.R. Bandy [1980].

"Concentration Distribution of Methyl Chloride in the Atmosphere," Jrnl. Geo. Res., 85, 7350, R.A. Rasmussen, L.E. Rasmussen, M.A.K. Khalil, and R.W. Dalluge, [1980].

"Atmospheric OCS Measurements on Project GAMETAG," Jrnl. Geo. Res., 85, 7357, A.L. Torres, P.J. Maroulis, A.B. Goldberg, and A.R. Bandy, [1980].

"Global Measurements of Aerosols in Remote Continental and Marine Regions: Concentrations, Size Distributions, and Optical Properties," Jrnl. Geo. Res., 85, 7361, E.M. Patterson, C.S. Kiang, A.C. Delany, A.F. Wartburg, A.C.D. Leslie, and B.J. Huebert, [1980].

"Variations of O('D) Photoproduction Rate for the 1977 GAMETAG Flights," Jrnl. Geo. Res., 85, 7377, Frederick A. Hanser, and Bach Sellers [1980].

"Iodine: Its Possible Role in Tropospheric Photochemistry," Jrnl. Geo. Res., 85, 7383, W.L. Chameides, and D.D. Davis [1980].

"Correlations Between H_2O and O_3 for the GAMETAG Vertical Sampling Tracks," D.D. Davis, D. Black, Kesheng Shau, M. Rodgers, Jrnl. Geo. Res., in preparation.

"A Theoretical Assessment of the GAMETAG Vertical Profiles for H_2O and O_3," W. Chameides, and D.D. Davis, Jrnl. Geo. Res., in preparation.

"Experimental Observations of Free Tropospheric OH Levels over the Sub-tropical and Tropical Pacific," D.D. Davis, M. Rodgers, D. Philen, W. Heaps, Jrnl. Geo. Res., in preparation.

"A Theoretical Assessment of the GAMETAG Free Tropospheric OH Measurements," W. Chameides, and D.D. Davis, Jrnl. Geo. Res., in preparation.

"C"

Global Tropospheric Chemistry:

A Proposal for a Coordinated Field Sampling Program

Prepared by:

The GAMETAG Executive Committee

Dr. D. D. Davis (Chairman)

Dr. C. S. Kiang

School of Geophysical Sciences
Georgia Institute of Technology
Atlanta, GA 30332

Dr. R. Duce

Graduate School of Oceanography
University of Rhode Island
Kingston, RI 02881

and Dr. P. Crutzen

National Center for Atmospheric Research
Post Office Box 3000
Boulder, CO 80307

EXECUTIVE SUMMARY

Recognizing the growing need to understand the chemical nature of the atmosphere, a six-year program is here being proposed which will have as its principal focus the troposphere. Designated GAMETAG II, this program has been designed with the purpose of substantially enhancing our present information base in three specific areas: (1) global concentration distributions of trace gases and aerosol species; (2) the relative distributions and magnitudes of natural global sources and sinks of atmospheric constituents; and (3) the further elucidation of reaction pathways which collectively define the chemical coupling between gas phase species as well as that with atmospheric aerosols. From this new information base it can be expected that there will result a significant improvement in our understanding of the global budgets of key elements that cycle through the atmosphere as well as the roles of numerous individual chemical species that participate in large scale planetary biogeochemical cycles. This information should prove to be of very fundamental importance to the on-going global assessment of the world's frequently conflicting needs for energy and environmental quality.

Representing a joint scientific venture between atmospheric chemists, meteorologists, marine chemists, and marine and terrestrial biologists, major participation in the GAMETAG II program will come from over thirty different universities, government laboratories, and private research institutes. Scientists from West Germany, Canada, and Mexico have also indicated a strong interest in participating, and it is now expected that scientists from additional countries will become involved during the final design stages of the program. In its present form, the GAMETAG II program is divided into three sub-phases. The first of these will involve coordination exercises, field testing of new airborne chemical sensors, and extensive calibration tasks. Phase IIA will require a time period of two and one-half years to be completed and will entail three short-term field operations. Phase IIB will encompass the major field sampling program element. It will involve two field operations over a two-year time period, each operation being two and one-half months in length. Phase IIC will define the final data reduction and analyses program element. A time increment of one and one-half years is now estimated for the completion of this final phase of the project.

The proposed GAMETAG II program is to be a "select" global tropospheric field sampling effort which will largely be concerned with sampling "representative" global regions of the unperturbed troposphere. Both continental and marine "representative" regions are to be included in the sampling format. Current planning calls for two, and possibly as many as three, airborne platforms plus two or more deep water oceanographic research vessels to be involved. Ground based field sampling stations will also be folded into the program whenever possible. Other key aspects of the GAMETAG II sampling strategy will include: (1) "simultaneous" temporal measurements of those trace gas species having short to moderate chemical coupling constants; (2) the use of the airborne meteorological correlation technique to measure in-situ fluxes of trace gas species found within the atmospheric boundary layer; and (3) the selection of flight scenarios that will maximize the number and types of measured tropospheric concentration gradients. The latter approach should especially serve to maximize the number of test points that can be generated for purposes of evaluating and upgrading current global tropospheric chemical models.

INTRODUCTION

The discipline of atmospheric chemistry can be broadly defined to include the study of the chemical composition of the atmosphere, its variability on a global scale, and studies of those major factors which collectively act to control atmospheric chemical composition; i.e., sources, sinks, chemical transformation rates, and atmospheric transport. Also falling within the domain of this discipline are studies of atmospheric chemical elements (i.e., S, N, C, and the halogens) which participate in large scale planetary biogeochemical cycles. From the above definition it should thus be evident that the field of atmospheric chemistry should be viewed as being strongly interdisciplinary in nature, depending on interactions with meteorologists, oceanographers, geologists, and biologists. The overlap with meteorology, in particular, has proven to be jointly beneficial to both disciplines. It has become increasingly clear, for instance, that the chemical composition of the atmosphere can have a significant influence on mesoscale and synoptic meteorological phenomena. This has been demonstrated to be particularly true for those microchemical processes which, in conjunction with microphysical events, influence precipitation patterns. Via scattering and/or absorption of solar radiation, the possibility also exists that atmospheric chemical composition may be responsible for long term fine tuning of planetary climate. The impact of meteorology on atmospheric chemistry is even more extensively documented. In this case it is well recognized that a clear definition of the transport characteristics of the atmosphere is of crucial importance to an understanding of the global concentration distributions of numerous trace gas and aerosol species.

During the last ten years there has been a rapid acceleration in the level of activity in at least two major areas of atmospheric chemistry. This activity can be correlated with two rather specific environmental

threats: urban pollution and stratospheric ozone depletion. Investigations of the "natural"* global troposphere have received much less attention. Increasingly, though, it is being recognized that there exists a very significant coupling between the troposphere and stratosphere and, furthermore, that man's rapidly expanding activities in the world are beginning to influence those areas of the troposphere once considered pristine. It thus appears to be increasingly important that a major coordinated scientific undertaking be initiated with the objective of improving our understanding of the "natural" troposphere. This information will undoubtedly prove to be of fundamental importance in our ultimately defining the much needed balance between world requirements for energy and environmental quality.

Some centers of global tropospheric activity can already be identified. These include the efforts of the international group SCOPE (Scientific Committee on Problems of the Environment) and its two closely working adjuncts GEMS (Global Environmental Monitoring System) and MARC (Monitoring and Assessment Research Center) and, within the U.S.A., the NSF (National Science Foundation)-sponsored programs SEAREX (Sea-Air Exchange) and GAMETAG (Global Atmospheric Measurements Experiment on Troposperic Aerosols and Gases). Although the primary objective of SCOPE and its adjuncts is strongly mission-oriented (e.g., defining both short and long term environmental threats on regional and global scales), considerable fundamental atmospheric work is being supported by these international groups in the area of ground-based global monitoring and studies of biogeochemical cycles. Project SEAREX, on the other hand, has been concerned with the exchange of gases and aerosols

* The term "natural", or alternatively "unperturbed", troposphere has been used here in the context of defining tropospheric regions where the concentrations of chemical species have not been significantly influenced by local or regional pollution sources. It is to be noted, however, that in the case of very long-lived species (e.g., CO_2, fluorocarbons 11 and 12), global atmospheric transport has already resulted in measured concentration levels which reflect a global impact from man's industrial activities.

between the oceans and the atmosphere, especially as coupled through long-range transport. Trace elements and high molecular weight organic materials have been of particular interest. Measurements of the fluxes of these substances both into and out of the ocean, as well as detailed studies of the exchange mechanism, have been emphasized. Project GAMETAG (also NSF-sponsored up to this point in time) has been directed toward obtaining more extensive information on the global concentration distributions of a broad spectrum of tropospheric trace gases and aerosol species. Also receiving central consideration in the latter program have been detailed studies of photochemical and non-photochemical transformation mechanisms. The findings from the Phase I GAMETAG program have resulted in seventeen major scientific papers.

The purpose of this document is that of outlining a second phase to the GAMETAG program. At the present time, scientists from over thirty different universities, government laboratories, and private research corporations have been identified for participation in this second generation global tropospheric chemistry effort. Three U.S.A. agencies have expressed strong support for this new initiative. Scientists from West Germany, Canada, and Mexico have indicated their intention to participate; and it is anticipated, with the writing of this document, that scientists from additional countries will also consider their involvement.

PROGRAM RATIONALE

Using as a guide the extensive scientific as well as operational knowledge gained from the GAMETAG I program, the authors have here outlined a second generation global tropospheric field sampling program. Its goal will be that of further enhancing our state-of-knowledge of global tropospheric chemistry. In formulating this new program, the authors have paid special attention to the fact that atmospheric chemistry, as an interdisciplinary field of study, is strongly dependent on an operational interaction with the fields of meteorology, oceanography, and biology. The success of this new field program is therefore perceived to be dependent on the formulation of a multi-disciplinary scientific team. Among those steps to be implemented in achieving this goal will be that of establishing working relationships between GAMETAG scientists and investigators involved in other global tropospheric research programs, i.e., SCOPE and SEAREX. Perhaps equally important could be establishing a strong interaction with biologists, chemists, and meteorologists located in those countries where field sampling is likely to occur. (The possibilities include: Mexico, Brazil, Argentina, Canada, Nigeria, Niger, Zaire, India and Australia).

Central to the GAMETAG II program will be measurements designed to add new information in three areas: (1) global concentration distributions of trace gases and aerosol species; (2) the relative distributions and magnitudes of natural global sources and sinks of atmospheric constituents; and (3) the further elucidation of reaction pathways which collectively define the chemical coupling between gas phase species as well as that with atmospheric aerosols. As noted earlier in the "Introduction", much of the information gathered in areas (1) and (2) will also require an assessment of the meteorological framework within which the GAMETAG chemical data are to be collected.

Concerning the first objective, it is recognized from the start that the GAMETAG II program will not be capable of providing a data base from which comprehensive global concentration distributions can be deduced. The proposed program is to be a "select" global tropospheric field sampling effort that will largely be concerned with sampling "representative" global regions of the unperturbed troposphere. The GAMETAG effort is therefore viewed by these authors as providing only a preliminary assessment of the global distributions of numerous trace gas and aerosol species. Even so, the data base generated will undoubtedly serve as a key planning element for future global field sampling programs. These futuristic programs could involve the use of satellites or shuttle platforms to obtain "blanket" coverage of large segments of the global troposphere.

Within the context of the three GAMETAG II program objectives defined above, numerous scientific questions will be addressed during the project. Representative of the types of questions to which partial and, in some cases, complete answers will be sought are the following:

(1) What are the relative roles of stratospheric-tropospheric exchange and photochemistry in controlling the global tropospheric ozone budget?

(2) What are the most important factors responsible for the measured higher carbon monoxide levels in the northern hemisphere versus those in the southern hemisphere (i.e., the intensity of anthropogenic sources, natural sources, or a combination of both)?

(3) What is the reliability of present free radical photochemical theory in predicting the distributions of trace atmospheric constituents in natural tropospheric air parcels?

(4) What is the yearly flux of sulfur now being released from the natural biosphere? What are the chemical forms of this sulfur? And, what are the global distributions of the different natural sulfur sources?

(5) What is the relative importance of homogeneous versus heterogeneous processes in the SO_2 gas-to-particle conversion cycle?

(6) What is the relative importance of lightning, stratospheric-tropospheric exchange, and continental and marine biospheric sources in defining natural tropospheric levels of NO_x?

In all, some thirty-five scientific questions have been formulated as the basis of the GAMETAG II program. Most importantly, this large listing is not perceived by us to be representative of the classical "shotgun" approach. Virtually all questions being put forward have some degree of overlap with other questions within the ensemble. Although recognizing that some trade-off decisions will still be necessary, it is generally believed that the extensive array of measurements to be made, in combination with the planned use of coordinated multiple sampling platforms, will provide an adequate basis for investigating this large array of questions. From a more pragmatic point of view, the GAMETAG I program has already provided ample evidence showing that the latter approach to studying global atmospheric chemistry does indeed result in the optimal scientific return for a given investment of resources.

PROGRAM STRATEGY

In its present form, the GAMETAG II program is to be divided into three sub-phases (see Fig. 1). Phase IIA will encompass four areas of activity: (1) coordinating exercises between the various types of sampling platforms; (2) field testing of new airborne chemical sensors, particularly those which are to be used in applying the airborne meteorological correlation technique for flux measurements; (3) field and laboratory inter-calibration exercises to identify possible systematic errors involving different sensor types measuring the same species; and (4) the testing of high-speed micro and mini-computer systems for purposes of demonstrating the feasibility of real time data analyses. This first sub-phase will require a time period of two and one-half years for completion and will entail three short-term field operations (see Fig. 1). Phase IIB will define the major field sampling program element. It will involve two field operations over a two year time period, each operation being two and one-half months in length. The third phase of the program, IIC, will encompass data reduction activities and detailed analyses of the results from Phase IIB. A time increment of one and one-half years is now estimated for the completion of this phase.

Concerning the details of the GAMETAG II sampling strategy, suffice it to say at this time that much of this strategy still remains to be worked out. However, several of the more important general characteristics of this new program initiative can be defined even at this early stage of the planning. In the text that follows, we have discussed these characteristics in the context of providing answers to four basic questions: Where to sample? When to sample? What to sample? And, how to sample?

With regard to the first question, as stated earlier, the major focus of the GAMETAG II program, like its predecessor GAMETAG I, will be the natural troposphere - to the extent that this is possible. It is recognized,

for example, that due to the fact that all operations will be initiated and terminated in the U.S.A., considerable amounts of sampling time will be expended which involve measurements in heavy to moderately polluted air parcels. This type of data, however, could prove to be of considerable value in the further assessment of the long-standing question related to the impact of industrial islands on remote regions of the troposphere.

Concerning sampling operations in the natural troposphere, it can be expected that larger amounts of sampling time will be expended in the southern versus the northern hemisphere. This decision is a direct reflection of the known lower pollution levels exhibited on the average in the southern hemisphere. For both hemispheres, though, the selection of "representative" regions will require still further evaluation. Suffice it to say, those natural continental and marine regions having the largest global area and the estimated greatest per unit area biomass productivity will receive the highest priority.

For Phase IIA, the general sampling region has tentatively been identified as the Yucatan peninsula and the surrounding marine areas consisting of the Gulf of Mexico and the Carribean Sea. This region has the advantage of close proximity to the U.S.A., suffers only slightly from long-range transport of pollution, and has both diverse marine and continental areas available for field testing of new instrumentation and sampling techniques.

The question of when to sample immediately brings to the forefront the more basic question: Should a large scale field program focus on sampling large numbers of "representative" regions or the sampling of a limited number of regions but with measurements spread out over two or more seasons of the year? As noted previously, such trade-off decisions can routinely be expected in any large field sampling project, and the proposed program will undoubtedly not be an exception. In this case, the authors

are proposing to focus on sampling a large number of different "representative" regions. The rationale here involves a consideration of both the limited duration of the major field sampling phase of the program (i.e., 2 years) and the paucity of data on sources, sinks and in-situ concentrations of species for most "representative" global regions. The possibility of obtaining some seasonal information, however, should still not be totally disregarded. In certain cases, for example, information on seasonal trends could possibly be deduced by sampling (during a given flight sequence) regions in both hemispheres having a similar biomass productivity and/or type of biological speciation.

The question of "what to sample" is again viewed by the authors as being of critical importance. It is the answer to this question that should dictate whether or not the GAMETAG II program is sufficiently advanced in its sampling technology to justify its inception at this point in time. In this regard, it is perhaps important to express one of the basic guidelines in designing the GAMETAG II program: Not all chemical measurements are viewed as being of equal importance in advancing the state of knowledge of tropospheric chemistry. Thus, the simplistic approach of measuring all things that can be measured has been discarded. Alternatively, a critical sub-set of species has been defined where the approach taken has involved examining each of the proposed GAMETAG scientific questions in the context of the chemical subcycles of H_xO_y, NO_x, carbon, sulfur, and halogen species. In this assessment, major consideration has been given to existing experimental data as well as reviewing the predictions of current theoretical models. This analysis has resulted in our estimating that a "critical set" of species would number approximately thirty-five; whereas, an "expanded critical set" of species would be closer to forty-nine. Although these numbers might appear formidable at first glance, it is most significant, we believe, that

during the GAMETAG I program a total of twenty-seven chemical species, along with ten physical/meteorological variables, were successfully measured (see Table I). In fact, a recent survey by these authors of new techniques now under development would suggest that virtually all of those species falling into the "critical" category could be measured by late 1983. Additionally, techniques capable of measuring several species falling into the "expanded critical set" could be expected to be available by the completion of Phase IIA.

Several factors are involved in answering the question of how to sample. During GAMETAG I, one of the overriding considerations was that of covering the maximum possible latitude range in each hemisphere. The objective in this case was that of assessing intra-hemispheric and inter-hemispheric concentration gradients for several tropospheric trace gases. These gradient measurements provided a unique set of test points for evaluating current atmospheric chemical models.

The GAMETAG II sampling strategy will involve a major expansion on the GAMETAG I strategy. Flight scenarios will be selected that will maximize both the number and types of concentration gradients measured. Representative of these will be: day vs. night sampling; boundary layer vs. free tropospheric sampling; flights before and after major precipitation events; flights across the ITCZ; sampling over contiguous continental areas having significantly different biomass density or biomass type; and measurements over contiguous continental and marine areas. Essential to carrying out this type of sampling format will be establishing several geographic logistics centers from which flight operations can be staged. Considering for the present time that there would be six to seven flights from each of these locations, this suggests that a total of four different logistic centers will need to be defined for each two and one-half month field operation.

Another important consideration in the GAMETAG II sampling strategy (as in GAMETAG I) will be the recognition that chemical species in the troposphere can be chemically coupled with time constants ranging from less than a second to time periods of months or years. When this coupling occurs in a day or less, simultaneous temporal measurements of the involved species is of crucial importance for understanding the respective concentration distributions. As the lifetime of a species is extended upward to weeks and months, the distribution of biospheric and/or atmospheric sources as well as atmospheric transport become of major importance in controlling a species' concentration distribution. In the latter case, the need for simultaneous measurements is significantly diminished. The nitrogen oxide sub-cycle shown in Fig. 2 illustrates a system that encompasses species falling into the first category. Based on current modeling studies of the several different sub-cycles of NO_x, H_xO_y, O_3, sulfur, and the halogens, it now appears that high resolution simultaneous temporal measurements will be required for a large percentage of those species that will be of interest to GAMETAG II program objectives.

A final point related to defining the GAMETAG II sampling strategy concerns the nature of the sampling platforms to be used. During GAMETAG I, only a single aircraft was employed, that being a four-engine Electra owned and operated by the National Center for Atmospheric Research. The shortcomings resulting from the use of this single aircraft, however, were found to be quite significant. In particular, it was found that the aircraft's limited altitude ceiling and limited flight range precluded the sampling of many tropospheric regions considered to be of major scientific importance. Additionally, the limited space afforded by this single aircraft platform prevented the installation of many chemical sensors capable of measuring other chemical species. In view of these limitations, present planning

would call for the participation in the program of at least two aircraft. The NCAR turbo-prop Electra, which is especially well suited to low altitude sampling, would be used predominantly to sample the atmospheric boundary layer and the lower free troposphere. A four-engine jet aircraft (i.e., the NASA-owned Convair 990) would then be stacked above the Electra and cover the middle and upper free troposphere. An overlap region involving the lower and middle free troposphere would be assigned to both aircraft for purposes of cross calibrating on-board chemical sensors. A third aircraft, again a turbo-prop Electra, is also being considered for purposes of providing a more extensive meteorological data base for each field sampling operation. If added, both on-board and in-situ meteorological sensors as well as drop-sondes would be employed for data collection. Radiosonde data from local and regional weather service stations will also form an important source of meteorological data. Collectively, the data from aircraft, local and regional radiosondes, and satellite observations will define the meteorological framework within which the chemical measurements are to be evaluated.

Although aircraft platforms will form the backbone of the GAMETAG sampling strategy, when sampling occurs over continental areas an extensive effort will be made to coordinate sampling flight tracks with known ground-based field sampling stations. In this context, a cooperative sampling effort with scientists in those countries or global regions designated for field sampling would prove to be a major asset to the proposed program. In the ground-based sampling effort, major emphasis would be placed on flux measurements, in-situ concentration measurements, and precipitation analyses. Of special interest in the ground-based sampling effort will be identifying stations that might provide time sequence data; that is, data collected before, during, and after the airborne measurements in the area. The latter type of data could significantly improve our understanding of the statistical reliability of the aircraft measurements.

For overflights in marine areas, a systematic effort will be made to coordinate major aircraft sampling exercises with those taking place on one or more oceanographic research vessels. Ocean water analyses (both chemically and biologically), surface air measurements, and precipitation analyses will be emphasized on these oceanographic platforms. Planning exercises with NOAA (National Oceanic and Atmospheric Administration) are presently getting underway in an effort to more fully explore these joint aircraft/ oceanographic research vessel sampling activities.

FIG 1: GAMETAG II TIMETABLE

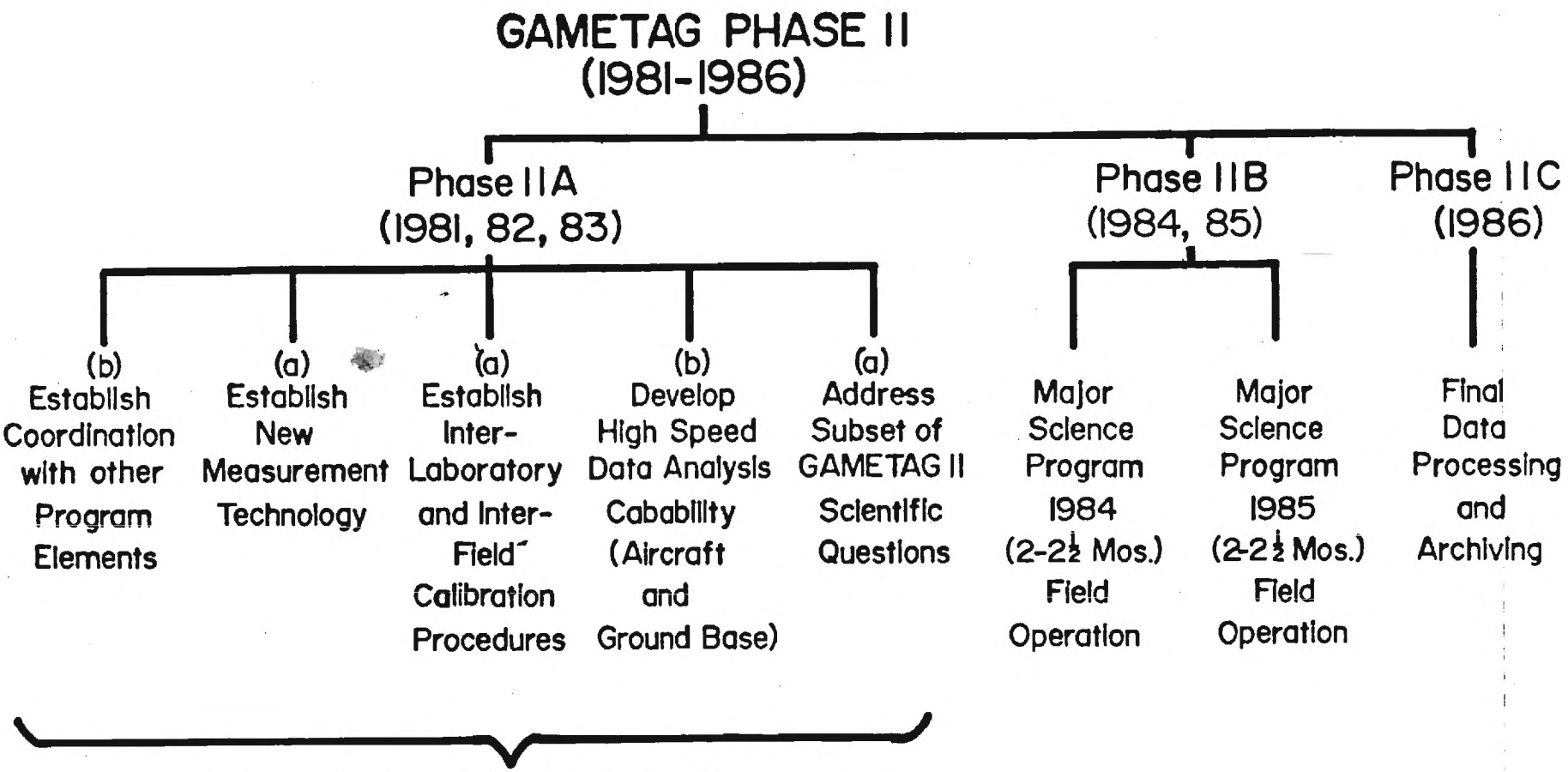

a) Highest Priority

b) Secondary Priority

FIG. 2: ONE OF SEVERAL POSSIBLE DAYTIME NITROGEN OXIDE CHEMICAL CYCLES

(REFERENCE: MARINE BOUNDARY LAYER)

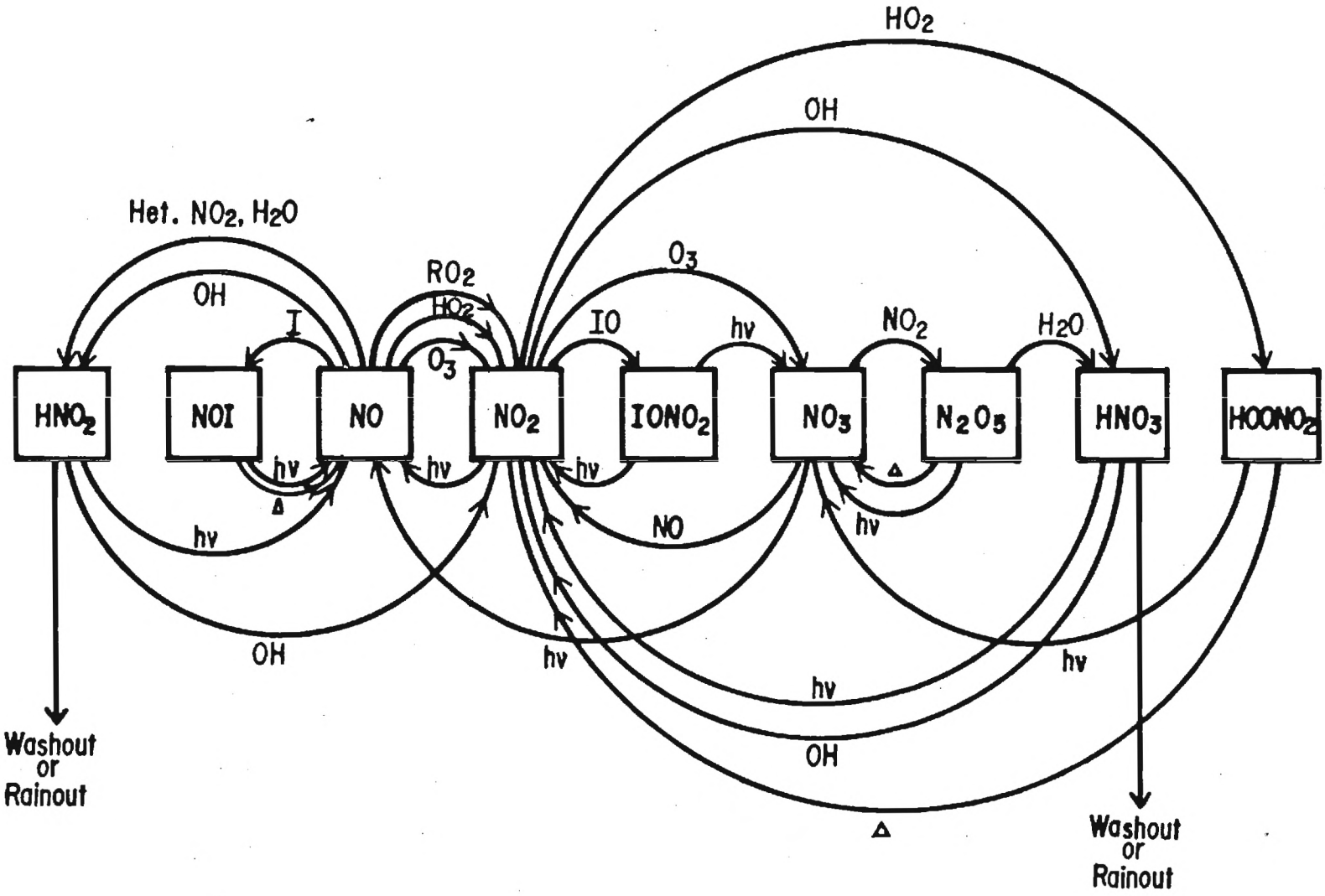

TABLE I

GAMETAG I MEASUREMENTS

VARIABLE MEASURED	TECHNIQUE
O_3	UV Absorption and Chemiluminescence
OH	Laser Induced Fluorescence
H_2O	Two Stage Thermo-electric Hygrometer
UV Flux	Ultraviolet Spectro-irradiometer
NO	Chemiluminescence
HNO_3	Filter Matte Collection-Wet Laboratory Chemical Analysis
NO_3^- SO_4^{-2} Cl^- NH_4^+	Filter Matte Collection-Wet Laboratory Chemical Analysis
Rn^{222}	Filter Matte Collection with on-board β Counting
SO_2 COS	Cryo Trapping with on-board GLC Flame Photometric Analysis
CO CH_3CCl_3 CCl_4 F-11 F-12	Air Stream Aliquot Sampling with on-board GC Flame Ionization and/or Electron Capture Analysis
CO CCl_4 CH_3CCl_3 F-11 F-12 CH_4	Grab Sampling Laboratory GC or GLC/ Flame Ionization and/or Electron Capture Analysis

VARIABLE MEASURED	TECHNIQUE
CH_3Cl C_2H_2 C_2H_4 C_2H_6 limited # H.M.W. hydro-carbons	Grab Sampling Laboratory GC or GLC/ Flame Ionization and/or Electron Capture Analysis
Aerosol Optical Properties	Polar Nephelometer
Aerosol Size/ Number Distr.	Knollenberg Spectrometers
Dew Point	Two Stage Thermoelectric Hygrometer
Air Temp.	Platinum Resistance Thermometer
IR Ground Emissions	Bolometric Radiometer
Broad Band Upward & Downward UV Flux	Broad Band Pyranometer
Pressure/ Altitude	Transducer

AIRCRAFT COMPUTED PARAMETERS
True Air Speed
Horizontal Winds
Vertical Gust Velocities
Geographical Position
Potential Temperature
Vertical Acceleration

Publications Related to Improved LIF OH Sensor

1. OH Rotational Quantum State Distributions and Relaxation Efficiencies for the Reaction System $O(^1D) + H_2O \rightarrow 2OH$; Chemical Physics Letters, 78, 246, [1981].

2. A Theoretical Assessment of the O_3/H_2O Interference Problem in the Detection of Natural Levels of OH via Laser-Induced Fluorescence; Geophys. Res. Lett., 8, 73 [1981].

3. An Experimental Assessment of the O_3/H_2O Interference Problem in the Detection of Natural Levels of OH via Laser-Induced Fluorescence; Geophys. Res. Lett., 8, 69, [1981].

Attachment "D"

Volume 78, number 2 CHEMICAL PHYSICS LETTERS 1 March 1981

OH ROTATIONAL QUANTUM STATE DISTRIBUTIONS AND RELAXATION EFFICIENCIES FOR THE REACTION SYSTEM $O(^1D) + H_2O \rightarrow 2OH$

M.O. RODGERS, K. ASAI and D.D. DAVIS
School of Geophysical Sciences, Georgia Institute of Technology, Atlanta, Georgia 30332, USA

Received 10 September 1980; in final form 10 December 1980

The OH rotational distribution from $O(^1D) + H_2O \rightarrow 2OH$ is presented. The $v'' = 0$ distribution corresponds to two Boltzmann distributions: $\approx$500 K ($k = 1-6$) and $\approx$2500 K ($k \geq 6$). Rotational relaxation efficiencies for N_2, He, O_2 were ≤ 0.1, ≤ 0.1, ≤ 0.4. More limited data are presented for the $v'' = 1$ and 2 levels.

1. Introduction

This report outlines experimental results related to defining the initial rotational quantum state distribution and subsequent relaxation of the products resulting from the reaction

$$O(^1D) + H_2O \rightarrow OH + OH, \quad \Delta H = -29 \text{ kcal/mole}. \tag{1}$$

An earlier report by Engleman [1] indicated that one of the OH radicals formed by reaction (1) is formed vibrationally cold, while the other OH product species is usually born vibrationally hot. Using isotopically labeled water, Engleman demonstrated that the OH species resulting from the newly formed H–O bond contained the excess vibrational energy. No detailed information was provided in the Engleman report on the OH rotational distribution resulting from reaction (1). This information is of both fundamental and practical importance. In the latter context, the nascent OH distribution from the $O(^1D)/H_2O$ reaction, and its subsequent relaxation, is of major importance in the application of the "laser-induced fluorescence" technique to the detection of natural atmospheric OH levels. We have addressed this point in greater detail in separate publications [2].

In this work, we examine the OH rotational distribution resulting from reaction (1) under conditions where, on the average, either no collisions occur or upwards of 25 collisions take place before the OH radicals are sampled. A discussion of these results and a comparison with other data recently reported [3], using a different experimental approach, are presented.

2. Experimental

The apparatus used in these experiments is shown in schematic form in fig. 1. Both O_3 photolysis and OH fluorescence pumping were achieved using a single frequency-doubled Quanta Ray PDL dye laser pumped by the second harmonic output of an ILS NT-674 Nd : YAG laser. With rhodamine 6G dye, UV energies up to 3 mJ/pulse could be obtained in the spectral range of 281–295 nm. For the experiments reported on here, energies of 160 μJ/pulse or less were typically used. UV pulses from the PDL system were shown to have a single transverse mode, a UV linewidth (calculated from visible measurements) of $\approx$0.001 nm, and a nominal pulse width of 7 ns. In our typical experimental apparatus, the UV beam from the frequency-doubled PDL was passed through a series of beam expansion telescopes and apertures, thus allowing only the central portion of the beam to be injected into the photolysis/fluorescence cell. This optical processing of the output beam was designed to ensure that any hot spots within the beam were significantly reduced in intensity relative to the surrounding energy field. Tests to evaluate the beam uniformity and to establish the absence of saturation effects were carried out by examining the

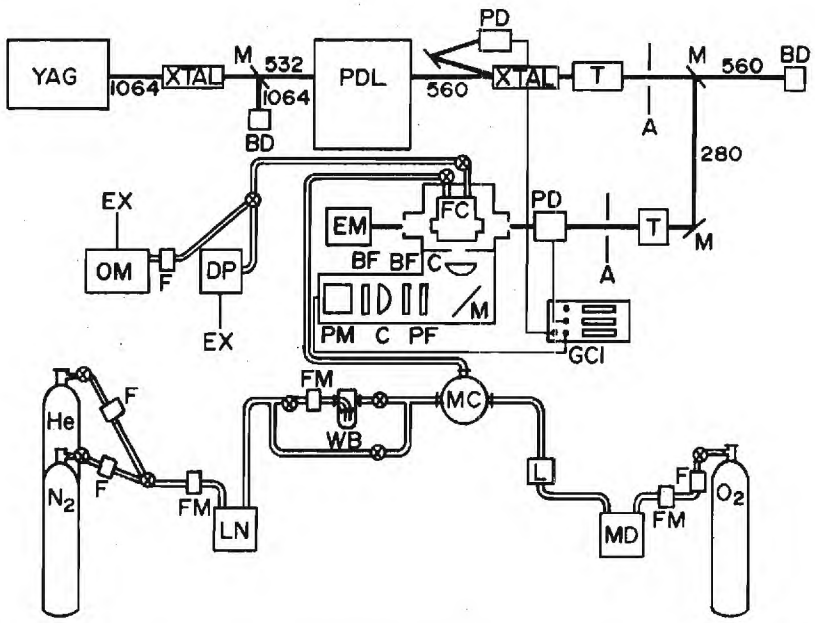

Fig. 1. Schematic diagram of an OH laser-induced fluorescence apparatus utilizing a slow-flow gas handling system. In this diagram, (A) aperture; (BD) beam dump; (BF) blocking filter ($\lambda > 400$ nm); (BP) band-pass filter; (C) collection lens; (DP) water vapor monitor; (EM) energy monitor; (EX) exhaust; (F) particle filter; (FC) fluorescence chamber; (FM) mass-flow meter; (GCI) gated charge integrator; (L) Hg lamp assembly, (LN) liquid-nitrogen trap, (M) mirror; (MC) mixing chamber; (MD) methanol, dry-ice trap; (OM) ozone monitor; (PD) photodiode; (PDL) dye laser; (PF) pyridine filter; (PM) photomultiplier tube; (T) telescope; (WB) water bubbler; (XTAL) doubling crystal; (YAG) Nd : YAG laser.

fluorescence signal resulting from the pumping of a single OH quantum transition as a function of the UV laser input energy. The energy range covered was 20–400 μJ. Within the experimental uncertainty of these measurements (i.e. ±10%), a square power dependence was found for both the high- and low-pressure experiments.

Additional tests to establish the absence of saturation were performed (principally at high pressure) by evaluating the relative signal strengths derived from different transitions originating from the same K level. (Oscillator strength variations ranged from a factor of 3–10). Results from these experiments were then compared to the known relative oscillation strengths for these same lines. On the average, the agreement between experiment and prediction was ±15%. The worst agreement was found to be 30%, with no bias toward low signal ratios indicating saturation. These collective results would thus seem to confirm the absence of significant saturation in these experiments.

In the above experiments, the absolute UV energy was measured periodically by either a Laser Precision pyroelectric UV monitor or a Scientech calorimeter. (In several cases, both were used in cross-calibration checks.) Continuous relative UV energy measurements were recorded using a photodiode assembly where a small fraction of the total laser energy was deflected into the diode by a beam-splitting mirror (see fig. 1).

The photolysis/fluorescence chamber consisted of an all-quartz vessel (volume = 0.6 ℓ) equipped with five input and/or output windows. Two high-vacuum teflon stopcocks attached to the vessel permitted the transfer of pre-mixed gas aliquots into the chamber for long-term experiments. Alternatively, the chamber could be connected into a slow-flow system (as shown in fig. 1) from which gas mixtures could be continuously varied over a wide range of compositions. Flow rates in this system were typically maintained in the 2.5–3.5 ℓ/min range at a total pressure of 1 atm.

The typical experimental gas mixture consisted of varying ratios of the gases O_2, O_3, N_2 and H_2O. However, a limited number of experiments were also carried out substituting He for N_2. Both the N_2 and He gases were Matheson UHP Gold Label. The gas

flows from both tanks were passed through a combination of traps: (1) a 1 μm particle filter, and (2) a liquid-nitrogen immersed glass-beam filled U-trap.

In the slow-flow sampling configuration shown in fig. 1, the O_2 and N_2 (or, alternatively, He) tanks were connected to the main flow line through linear-mass flow meters (Teledyne Hastings models NALL-5k and AHK-5x). The N_2 gas stream was further partitioned between two secondary lines: one being directed into an H_2O bubbler, the other acting as a by-pass line. The N_2 flow in each of these lines was controlled by a series of precision needle valves; thus, depending on the flow rate through the H_2O bubbler, H_2O levels in the photolysis/fluorescence cell could be adjusted over the range of 0.2–18 Torr.

Ozone in the slow-flow system was generated by the 185.9 nm photolysis of O_2. The O_2 gas used in these experiments was Matheson UHP Gold Label. Additional cleaning of this gas stream was achieved by flowing the gas through tandem traps consisting of a small particle filter and a glass-bead filled U-trap held at dry-ice/methanol temperatures. Adjustments in the 184.9 nm flux and the O_2 flow rate could be used to achieve O_3 concentrations in the 20–2000 ppbv range. The resulting O_2/O_3 gas mixture was combined with the N_2/H_2O gas stream in a mixing chamber as shown in fig. 1. The final gas mixture, consisting of O_2, O_3, N_2 and H_2O, passed through the photolysis/fluorescence chamber and then entered either an O_3 or H_2O sensor. Both gases were monitored alternately for several minutes during each experimental run until stable levels of each could be defined. The O_3 monitor consisted of a Dasibi model 1003-AAS instrument which was calibrated over the range of 2–4000 ppbv.

Reliable measurements of the H_2O concentration level proved to be somewhat more difficult than those for O_3. Four different techniques were used in checking H_2O levels over the operational range of 0.2–18 Torr. In the first technique (useful from 0.2 to 6 Torr), mass-flow meters were used to record flow rates in both the N_2 by-pass and the N_2/H_2O bubbler lines. In this case, the final H_2O level could be calculated assuming the N_2 gas leaving the bubbler was saturated (an assumption proven to be true, particularly for high flow rates through the bubbler). Two commercial instruments were also installed in the flow system for purposes of making direct H_2O (actually relative humidity) measurements. The first of these devices consisted of a capacitance-type humidity indicator (Weathermeasure model HM-111, useful over the range of 2–18 Torr); the second was a thermoelectric frost-point hygrometer (EG&G model 140-C1). The frost-point hygrometer, in particular, provided consistent results over the entire H_2O range (0.2–18 Torr) covered in our experiments. The last method used in H_2O determinations was that involving the monitoring of 184.9 nm extinction through a 1.5 m optical cell in the N_2/H_2O flow line. The latter method was again quite effective at higher H_2O levels (3–18 Torr). Cross calibrations between these various instruments showed agreement to ±5% for the H_2O range of 3–18 Torr and ±10% over the range of 0.2–3 Torr.

In a typical experiment, the frequency-doubled output from the PDL dye laser was injected, after beam conditioning, into the photolysis/fluorescence chamber wherein $O(^1D)$ atoms were formed by the UV photolysis of O_3, i.e.

$$O_3 + h\nu \rightarrow O(^1D) + O_2, \quad (2)$$

followed by either

$$O(^1D) + M \rightarrow O(^3P) + M^*, \quad (3)$$

or

$$O(^1D) + H_2O \rightarrow OH + OH. \quad (4)$$

Available data [4] show that over the wavelength range of interest (280–295 nm) the $O(^1D)$ quantum yield is $\leqslant 0.85$. Upon formation of OH radicals by reaction (4), fluorescence pumping of the $X\,^2\Pi$ - $A\,^2\Sigma^+$ OH transition was achieved by the absorption of an additional UV photon from the remainder of the laser pulse. Thus, the outlined detection scheme requires the absorption of two photons from the same laser pulse.

Since tuning over a rather broad spectral range was required to sample all OH "k" levels, the above approach necessarily required that all fluorescence signals be adjusted to account for changes in the O_3 absorption cross section with wavelength. This rather broad spectral tuning range also raises the question of the wavelength dependency of the sampling optics. This potential problem was examined by testing several different k levels (both high and low states) where the optical pumping wavelength was varied by as much as 1.8 nm. These experiments were performed both with

and without a 10 nm (fwhm) band-pass filter centered at 310 nm. The results, in this case, showed little or no sampling discrimination. Thus, for purposes of maximizing the signal/noise ratio, in most experiments the 10 nm band-pass filter was inserted in the optical sampling train.

The fluorescence resulting from the laser-induced excitation of OH radicals was collected and detected by an optical train consisting of two quartz lenses, three filters, and an RCA 8850 PMT. Details on this system and the signal processing electronics have been previously described [5] and will not be further discussed here.

Since, as noted earlier, the fluorescence signal in our system depends on the square power of the UV energy (for constant beam diameter), every effort was made to carry out a complete set of k-level measurements using a constant laser energy. In actual fact, some energy variations could not be avoided; but the final correction required due to energy variations was typically held to ±15%.

After the above corrections were taken into consideration, the raw fluorescence signal measurements for each k level were converted into an OH population number by dividing by the corresponding Einstein B coefficients [6]. Signals were also corrected for changes in the electronic quenching environment due to changes in the H_2O vapor concentration. This correction, however, did not influence the calculated relative populations. It should be noted that throughout this study we have assumed the fluorescence efficiency, including the effects of electronic quenching and radiative lifetime, did not measurably change with the k level over the quantum state range of $k = 1$–15. Recent work by German [7] would seem to justify this assumption at least for low k levels. Further tests are now being planned to verify this assumption for the higher k levels.

3. Results and discussion

The majority of the results reported here are related to measurements of the OH rotational distribution within the $v'' = 0$ manifold for OH radicals formed by reaction (1). The principal spectroscopic branch examined was the R branch corresponding to the (1,0) band of the $X\,^2\Pi \rightarrow A\,^2\Sigma^+$ electronic transition. The R branch was chosen for this investigation due primarily to its relative freedom from interfering satellite lines and degeneracies. Experiments involving the $v'' = 1$ and $v'' = 2$ manifolds were carried out by pumping the (2,1) and (3,2) bands of the $X\,^2\Pi \rightarrow A\,^2\Sigma$ transition. Limitations in the use of these transitions were encountered, however, due to predissociation occurring at relatively low k levels in the excited state.

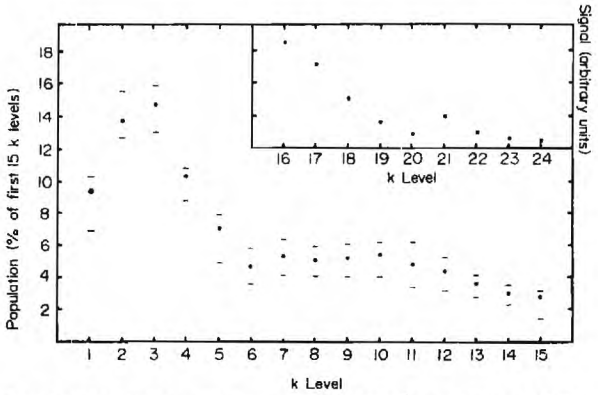

Fig. 2. Rotational quantum state distribution ($v'' = 0$) of OH radicals formed from reaction (1). Average of 15 R_1 branch distribution experiments (i.e., ≈225 individual measurements) for a gas mixture of: $[N_2]$ ≈580 Torr; $[O_2]$ ≈150 Torr, $[H_2O]$ = 16.5 Torr typical; $[O_3]$ = 2000 ppbv typical; laser energy = 160 μJ/pulse (10 or 0.03 pps) typical. Horizontal bars indicate approximate 2σ error limits. Inset represents normalized signals (arbitrary units) recorded for $k \geqslant 16$.

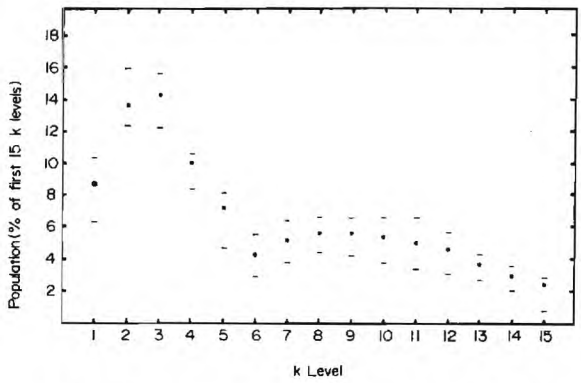

Fig. 3. Rotational quantum state distribution ($v'' = 0$) of OH radicals formed from reaction (1). Average of 3 R_1 branch distribution experiments (i.e., ≈45 individual measurements) for a gas mixture of: $[O_2]$ = 5 Torr; $[H_2O]$ = 400 mTorr, $[O_3]$ = 1 Torr; laser energy = 160 μJ/pulse (0.03 pps) typical. Horizontal bars represent approximate 2σ error limits. Error limits are similar to fig. 2 due to higher signal-to-noise ratios in these experiments.

Figs. 2 and 3 provide a summary of the results for the R branch experiments involving two extreme sets of experimental conditions: (1) OH formation in the presence of 1 atm of N_2, and (2) OH formation at very low total pressures (i.e., ≈5 Torr of O_2). In each case, it can be seen that the population plots appear to be the result of a superpositioning of two distinct distributions. In both figures, the first 15 k levels have been presented in terms of percent of total population; thus, the relative populations given are based on these first 15 k levels defining 100% of the OH rotational distribution in the $v'' = 0$ manifold. In fact, fluorescence signals were observed up to $k = 24$ even though at $k = 16$ predissociation in the excited state became apparent. In fig. 2, the relative fluorescence signal (in arbitrary intensity units) has been presented in the upper right hand corner of the plot for $k > 16$. The quantitative assessment of the $k > 16$ population was made difficult by the previously mentioned predissociation problem. It would appear quite significant, however, that no fluorescence signal could be observed for $k = 25$ and 26 in the $v'' = 0$ manifold. If the full exothermicity of reaction (1) were to appear predominantly as rotational excitation, $k = 24$ would correspond to the highest k level capable of being populated. Experiments were also performed utilizing the P and Q branches. In all experiments, selected satellite lines were compared to their respective principal lines to evaluate possible saturation effects and to examine the Λ doublet states. The results of these experiments may be summarized by three general findings: (1) the P and Q branch experiments gave the same type of distribution illustrated by figs. 1 and 2; (2) the satellite experiments demonstrated that no saturation effects were present, and (3) both the P and Q branch and the satellite line experiments indicated a slight (≤1.2×) non-statistical distribution between the two Λ doubling components, with the lower state being more populous.

Fig. 4 presents a surprisal plot derived from the population data given in fig. 2. Although no surprisal plot has been given here for the data shown in fig. 3, quite obviously the latter distribution results in a plot which closely resembles that of fig. 4. Because of the apparent two-distribution profile shown in fig. 2, an effort has been made in fig. 4 to resolve these data into two separate linear surprisals. In each case, the curves can be identified in terms of population distributions corresponding to temperatures of 500 ± 75 and 2500 ± 500 K. These results suggest, but do not prove, that the low k-level distribution may be related to the OH radical derived from the original O–H bond in H_2O; whereas, the high k-level distribution corresponds to the newly formed O–H bond.

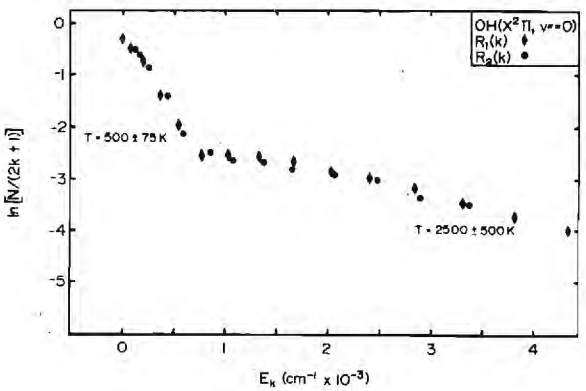

Fig. 4. Surprisal plot of R_1 and R_2 data. The experimental conditions are the same as those specified for fig. 2. A best fit of all data corresponding to $k = 1-6$ indicates a rotational temperature of 500 ± 75 K (2σ error limit). The data for $k = 7-15$ corresponds to a rotational temperature of 2500 ± 500 K (2σ error limit).

Gericke et al. [3] have examined reaction (1) at low pressure using laser absorption spectroscopy. These authors have reported that the distribution of OH from $k'' = 1-6$ was best represented by a Boltzmann distribution with a temperature of ≈480 K (for their R branch measurements). For levels $k > 7$, they reported "strong deviation" from a 480 K distribution. Smith et al. [8] have reported preliminary results on the OH distribution from reaction (1). The results of Smith et al. [8] have been qualitatively described by Lin [9] in terms of a k-level population corresponding to a temperature of at least 2000 K. Details on the latter study, however, are not yet available.

Our data on the R_2 branch, also shown in fig. 4, suggest that, within the experimental uncertainty of our measurements, the R_1/R_2 ratio is consistent with the hypothesis that the OH formed in the $v'' = 0$ manifold from reaction (1) is statistically distributed between its two possible spin states.

Of considerable importance in this study were measurements designed to show the degree of rotational relaxation which might occur during the 7 ns laser

pulse. Based on simple collision theory, it can be calculated that, on the average, ≈20 collisions could be expected to take place between N_2 (at 1 atm) and OH before the average OH radical species might be sampled. Under our low-pressure conditions (fig. 3), the average OH radical would make less than one collision with O_2. From an examination of figs. 2 and 3, it can be seen that no dramatic shift in the OH k-level distribution occurred as a result of the enhanced N_2 collision environment. Additional experiments performed at 1 atm N_2 and H_2O levels which varied from 0.2 to 18 Torr also resulted in no dramatic deviations in the measured OH k-level distribution within the sampling time of 7 ns. Finally, profiles determined under conditions of 1 atm of He (substituted for N_2) revealed no major differences in the rotational distribution. These results suggest that for such stable gases and He, N_2, and O_2, the collision efficiencies for k levels ≥ 5 are probably no greater than 0.1, 0.1, and 0.4, respectively. It is to be noted that the above qualitative results are not altogether surprising. Other investigators [10] have indicated that typical ground-state rotational relaxation efficiencies are in the range of 0.05–0.1. Our results also suggest that H_2O cannot be more than 40 times more efficient than N_2 in rotational quenching of OH. More quantitative studies of these relaxation rates (involving N_2, O_2, He or H_2O as collision partners) are now being planned using a double-pulsing laser system having a variable coupling time delay.

Quantitative measurements of the rotational distribution in the $v'' = 1$ and $v'' = 2$ manifolds, using our technique, were made quite difficult due to predissociation which occurred at low k levels in both the $v' = 2$ and $v' = 3$ manifolds of the excited state. Even so, very significant fluorescence was observed from pumping low and intermediate k levels in the $v'' = 1$ manifold and also from the low k levels in the $v'' = 2$ manifold. These observations are consistent with the results obtained earlier by Engleman [1], who reported the existence of vibrationally excited OH radicals arising from reaction (1). A qualitative estimate of the rotational distribution of the $v'' = 1$ state suggests that this distribution may be approximated by a rotational temperature of 2000–3000 K. No estimates of the distribution of the $v'' = 2$ manifold were possible.

4. Conclusions

We report here the results from experiments designed to show the rotational quantum state distribution for OH radicals formed by reaction of $O(^1D)$ with H_2O. These results indicate that the rotational distribuiton within the $v'' = 0$ manifold of the ground state may be approximated by a superpositioning of two Boltzmann distributions. The first distribution, valid for the region $k'' = 1$–6, corresponds to a rotational temperature of ≈500 K. The other distribution, valid for higher k levels, corresponds to a rotational temperature of ≈2500 K. Qualitative estimates of the $v'' = 1$ distribution suggest a single rotational distribution corresponding to a temperature of 2000–3000 K. Isotopic substitution experiments are planned to establish the relative populations within each k level arising from the OH formed by the new O–H bond and that arising from the existing O–H bond in H_2O.

Little or no rotational relaxation was observed in the high-pressure experiments during the time period of the laser pulse, i.e. 7 ns. These results suggest that an upper limit on the rotational relaxation efficiency for He and N_2 would be 0.1, and that for O_2 would be 0.4. The upper limit on the relative collision efficiencies of H_2O/N_2 was indicated to be no more than 40 : 1.

Acknowledgement

DDD acknowledges partial support of this research by the National Science Foundation (Grant ATM-~~8007481~~ 8123598). He also thanks Mr. Steve Fischer and Ms. Leah Turner for their assistance in the collection of experimental data and Drs. A.R. Ravishankara and Paul H. Wine for the use of their high-purity gas handling system for portions of this research.

References

[1] R. Engleman Jr., J. Am. Chem. Soc. 87 (1965) 4193.
[2] D.D. Davis, M.O. Rodgers, S.D. Fischer and K. Asai Geophys. Res. Letters, to be published;
D.D. Davis, M.O. Rodgers and S.D. Fischer, Geophys. Res. Letters, to be published.
[3] K.H. Gericke, G. Ortgies and F.J. Comes, Chem. Phys. Letters 69 (1980) 156.

[4] R.K. Sparks, L.R. Carlson, K. Shobatake, M.L. Kowalczyk and Y.T. Lee, J. Chem. Phys. 72 (1980) 1401;
D.L. Philen, R.T. Watson and D.D. Davis, J. Chem. Phys. 67 (1977) 3316.
[5] D.D. Davis, W.S. Heaps, D. Philen, M. Rodgers, T. McGee, A. Nelson and A.J. Moriarty, Rev. Sci. Instr. 50 (1979) 1505.
[6] W.L. Dimpfl and J.L. Kinsey, J. Quant. Spectry. Radiative Transfer 21 (1979) 233.
[7] K.R. German J. Chem. Phys. 62 (1975) 2584.
[8] G.L. Smith, J.E. Butler, L.D. Talley and M.C. Lin, National ACS Meeting, Washington, D.C. (1979).
[9] M.C. Lin, private communication (1980).
[10] G.D. Downey, D.W. Robinson and J.H. Smith, J. Chem. Phys. 66 (1977) 1685;
D.E. Pritchard, N. Smith, R.D. Driver and T.A. Brunner, J. Chem. Phys. 70 (1979) 2115,
I. Procaccia and R.D. Levine, J. Chem. Phys. 64 (1976) 808.

Attachment F

GEOPHYSICAL RESEARCH LETTERS, VOL. 8, NO. 1, PAGES 69-72, JANUARY 1981

An Experimental Assessment of the O_3/H_2O Interference Problem in the Detection of Natural Levels of OH Via Laser Induced Fluorescence

D.D. Davis, M.O. Rodgers, S.D. Fischer, and K. Asai

School of Geophysical Sciences
Georgia Institute of Technology
Atlanta, GA 30332

Abstract. Using simulated tropospheric conditions in a laboratory study as well as OH field measurement data from project GAMETAG (Global Atmospheric Measurements Experiment on Tropospheric Aerosol and Gases), an experimental assessment has been completed of the $O_3/H_2O/OH$ laser induced interference problem. These results indicate that, for the tropical marine boundary layer, the OH interference level averaged ~38% during the GAMETAG field measurements program. The average "useable" UV laser energy employed in these boundary layer OH measurements was 165 μJ. OH interference estimates in the case of the free troposhere were substantially lower, being ~13% for an average "useable" UV laser energy of 250 μJ. Modelling calculations suggest that the existing $O_3/H_2O/OH$ interference problem could be reduced still further, by factors of five to six, through the use of very narrow UV laser pulses (i.e., .5 to 1 ns vs. 7 ns).

Introduction

It has been pointed out in an adjacent paper that three approaches may be taken in evaluating the potential problem of $O_3/H_2O/OH$ interference in the measurement of natural levels of tropospheric OH via the LIF technique. The first of these, i.e., theoretical calculations of the OH interference signal, has been presented (see Davis, et al., this issue of GRL). The second and third approaches, involving laboratory measurements of the OH interference signal under simulated atmospheric conditions and the use of OH field measurements, are the subject of this paper.

Heretofore, the laboratory approach has fallen short of providing the required information on OH interference signal levels. The major problem in these studies has been that of reaching atmospheric conditions in a laboratory chamber without generating concomitantly unworkable noise levels. In this study this difficulty has been overcome with the fabrication of a slow-flow gas handling system and the acquisition of a more versatile and stable tunable dye laser.

Experimental

The experimental details on the slow-flow gas handling system, as well as the new pulsed-dye laser system, have been described elsewhere (Rodgers, et al., 1980); thus, only the most relevant experimental features of these two new systems will be given here.

Both the UV photolysis of O_3 and the subsequent excitation of $O(^1D)/H_2O$ generated OH were achieved using a single laser pulse from a frequency-doubled Quanta Ray-PDL dye laser. The latter system was pumped by the 2nd harmonic output of an ILS NT-674 Nd:YAG laser. The UV pulses from the PDL system were shown to have a single transverse mode, a UV line width (calculated from visible measurements) of ~.001 nm, a nominal pulse width of 7 ns, and an average beam diameter (after optical conditioning) of 8 nm. These characteristics were very similar to those described for an earlier dye laser system (Davis, et al., 1979; Davis, et al., 1980). The average energy used through the laboratory study was 170 μJ. Flow rates in the photolysis/fluorescense system were typically maintained in the 2.5 to 3.5 l/min range at a total pressure of one atmosphere. Gas mixtures consisted of varying ratios of O_2, O_3, N_2 and H_2O. The O_2 and N_2 filling lines were connected into the main flow line through linear-mass flow meters (Teledyne Hastings Model NALL-5k and AHK-5X). The N_2 gas stream was further partitioned between two secondary lines: one being directed into an H_2O bubbler, and other acting as a by-pass line. Depending on the flow rate through the H_2O bubbler, H_2O levels in the photolysis/fluorescense chamber could be adjusted over the range of .2 to 18 Torr.

Ozone in our system was produced by the 184.9 nm photolysis of O_2. Adjustments in the 184.9 nm flux or the O_2 mass flow rate could be used to achieve steady O_3 concentrations in the 20 to 2000 ppbv range. Both O_3 and H_2O were monitored alternately for several minutes during each experimental run until stable levels of each could be defined. For further details on the H_2O and O_3 sensors see Rodgers, et al., 1980.

One of the important characteristics of the slow-flow system employed in this study was the accuracy with which the photolysis/fluorescence chamber noise level could be defined. In this system the noise could be accurately measured by simply reducing the O_3 level in the flowline to zero, the latter being achieved by turning off the 184.9 nm Hg light source. In combination with long integration times (a feat possible because of the high degree of stability shown by the new PDL laser), signal-to-noise ratios of 1:500 per laser shot were recoverable.

Throughout the laboratory $O_3/H_2O/OH$ interference experiments, the principal OH transition used was that corresponding to the $Q_1(1) \rightarrow X^2\Pi - A^2\Sigma^+$ transition centered at 281.9 nm. This is the same transition used in all of our past OH field studies.

The collection optics and PMT employed in the laboratory atmospheric simulation study were nearly identical to those used in previous field studies (see Davis, et al., 1979), the major difference being the number of PMT's used (i.e., 1 versus 6 in the field). In addition, small differences existed in the bandpass filter as well as in the geometric spacing between the fluorescence zone and the first collection lens. For a single PMT, this resulted in an optical collection efficiency factor for the laboratory which was 1.20 times higher than for the aircraft set-up.

Results and Discussion

Laboratory Studies:

Earlier efforts by this group to perform laboratory OH interference experiments were shown to be of only limited value since the magnitude of the crucial concentration product $[H_2O] \times [O_3]$ was 200 to 1000 times higher than encountered in the clean troposhere (e.g., the tropical-marine boundary layer). In the present study, gas compositions have been attained which simulate the tropical-marine boundary layer in terms of N_2, O_2, O_3, and H_2O. The laser parameters chosen also duplicate those previously employed in field studies.

Results from the laboratory study are presented in the form of Fig. 1. In this diagram we have plotted the concentration product $[O_3] \times [H_2O]$ as a function of the measured fluorescence signal, based on a 10-minute integration time. Note, however, that in several experiments, involving the lowest values of the product $[O_3] \times [H_2O]$, much longer integration times were required to get a 3:1 or better signal-to-noise ratio. For the lowest point on the curve, the O_3 concentration was 20 ppbv and the H_2O level wa 17 Torr.

Experimental runs at very high $[O_3] \times [H_2O]$ product levels (i.e., 2.5×10^5) were also found to lie within (±10%) of the line drawn from the data points shown in Figure 1. Considering all data points, the average deviation from the straight line drawn in Fig. 1 was ±15%, and the worst deviation ±30%.

Paper number 80L1580.
0094-8276/81/0080L-1580$01.00

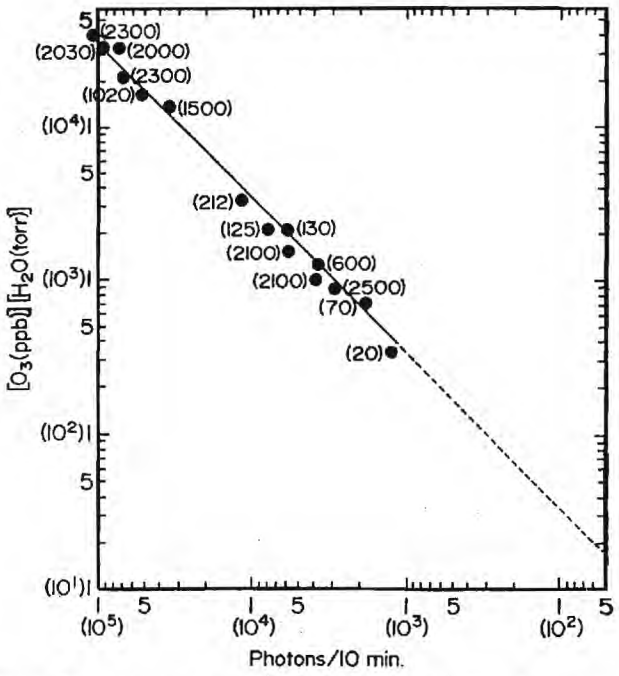

Fig. 1: Fluorescence interference signal (photons/10 min.) versus $[0_3] \times [H_20]$ for a laser energy of 170 μJ and a laser pulse width of 7 nm (FWHM). All signals are normalized for electronic quenching effects using $N_2/0_2/H_20$ relative electronic quenching efficiencies of 1/4/25, respectively (normalization conditions: $[0_2]$ = 160 Torr; $[N_2]$ = 590 Torr; $[H_20]$ = 17 Torr). Numbers in parentheses represent the 0_3 concentration for each experiment in units of ppbv. The straight line drawn through the data points represents a weighted least squares fit of the data where the weighting factor was defined by the number of individual experimental runs carried out for each set of 0_3 and H_20 conditions.

From an examination of Fig. 1 it can be seen that, for an $[H_20] \times [0_3]$ product level corresponding to the tropical marine boundary layer and for an input energy of 170 μJ, ~1100 fluorescence photons/10 min. were measured. This interference signal can be directly compared with the fluorescence signal derived from a natural 0H source, using the same laser parameters and the same collection optics. The appropriate expression is:

$$(I)\quad \frac{(0H_{Interf.})_{Fluor.}}{(0H_{Nat.})_{Fluor.}} = \frac{(0H_{Interf.}\text{Photons/10 min.})_{Lab\ Expt.}}{[0H_{Nat.}] \times (0H_{Nat.}\text{Signal Calib. Factor/10 min.}) \times (E_{Interf.}/E_{Calib.})}$$

where the term $(0H_{Interf.}\text{Photons/10 min.})_{Lab.\ Expt.}$ represents the number of fluorescence photons derived from the laboratory interference experiments for marine-boundary layer conditions (taken from Fig. 1), and the product $[0H_{Nat.}] \times (0H_{Nat.}$Signal Calib. Factor/10 min.) represents the number of detected fluorescence photons resulting from a known concentration of 0H (representative of a Boltzmann distribution at ~298 K), again for an integration time of 10 min. The calibration factor in this system (for a 10 nm bandpass filter centered at 309.5 nm) has previously been measured in our lab to be 2749 per 10^7 OH's per 10 minute integration time. This calibration number was established by photolyzing known mixtures of N_2, H_2, and H_20 with a well characterized 184.9 nm Hg lamp (Davis, et al., 1979, 1980b). The calibration factor quoted also reflects the effects of 0_2, N_2, and H_20 quenching of OH fluorescence. The quenching efficiencies for 0_2 and H_20, relative to N_2, were 4:1 and 25:1, respectively (Davis, et al., 1980b). The collection optics in the lab calibration experiments were the same as in the lab 0H interference measurements. The remaining two terms in equation (I), $(E_{Calib.})$ and $(E_{Interf.})$ represent the average laser energy used in each experiment. These values were 184 and 170 μJ, respectively.

Using the above cited values for $(0H_{Interf.})$, $(0H_{Signal\ Calib.\ Factor})$, $(E_{Calib.})$, and $(E_{Interf.})$ and taking the natural 0H level to be $10^7/cm^3$ (Chang, et al., 1978; Chameides, private communication), the ratio of the interference signal to the natural 0H signal is calculated from equation I to be .43 (for tropical-marine boundary layer conditions). This represents a 30% interference correction based on 170 μJ of useable laser energy. A comparison of this result with that derived from earlier theoretical calculations (for the same natural OH level) can be made if the lab experiments are adjusted for the difference in laser energy, i.e., 170 μJ vs. 165 μJ. This comparison shows the lab experiments predicting a 30% interference; whereas, the theoretical calculations suggest a 51 to 62% interference (based on the square-wave model). A similar comparison for the tropical-marine free troposphere (~5.5 km) can be carried out provided one takes the 0H interference signal level predicted from an extrapolation of the data shown in Fig. 1 and provided the $0H_{Nat.}$ calibration factor and the 0H interference signals are both increased by a factor of 2.8 due to a decrease in fluorescence quenching by 0_2, N_2, and H_20. In addition, both signals must be scaled to an energy of 250 μJ. (Scaling of the calibration signal goes as 250/184; whereas, that of the $0H_{Interf.}$ signal would go as 250/170.). Finally, a natural free-tropospheric midday 0H level of $2.5 \times 10^6/cm^3$ (Chang, et al., 1978 and Chameides, private communication) is to be introduced into equation I. From these adjustments a free-tropospheric interference level of 13% is estimated. This can be compared with our earlier theoretical predictions of 25 to 35%. The lab vs. theoretical approaches thus differ by a factor of 1.8 to 2.1 for the boundary layer and 1.9 to 2.6 for the free troposhere. The somewhat larger deviation for the case of the free troposphere may reflect errors resulting from the extrapolation of the data in Fig. 1 to free-tropospheric conditions.

Field Measurements:

As noted in the "experimental" section, the one major difference between the 0H lab interference set-up and the 0H field-sampling probe was the number of PMTs used. Small differences existed in the relative efficiency of the two sets of collection optics, due primarily to differences in the geometric sampling arrangements, and to the transmission characteristics of the bandpass filters centered at 309.5 nm. Taking the above collection efficiency factors into consideration (i.e., net 1.20 in favor of the lab system), photon fluorescence signals from the lab OH interference study can be compared (after normalizing for energy differences) with fluorescence signals recorded under field-sampling conditions. Since the 0H interference signal depends on the square power of the energy (for constant beam diameter), the energy normalization is given by the ratio $(E_{Interf.}/E_{Field})^2$. Due, however, to the fact that most boundary-layer field measurements were recorded at energies near 170 μJ, this normalization factor was typically found to be small.

The principal set of field data used in this comparison are those resulting from project GAMETAG (Global Atmospheric Measurements Experiment on Tropospheric Aerosols and Gases). In Table I we have summarized the interference level for several GAMETAG tropical-marine boundary-layer 0H measurements. For each set of field conditions (i.e., $[H_20] \times [0_3]$), the corresponding 0H interference signal has been estimated from Fig. 1 and the results then adjusted for differences in laser energy, sampling collection efficiency, and the number of PMTs used. However, no laboratory 0H calibration factor is required in this evaluation. Based on representative GAMETAG data, the range of the 0H interference correction is seen to be 22 to 54%, giving an average percent interference of 38%. The somewhat higher interference level calculated from the field measurements, relative to the laboratory evaluation, may be due, in part, to the slightly lower average concentration value measured for tropical boundary layer OH, i.e., $8.5 \times 10^6/cm^3$ vs. the previously assumed value of 1×10^7.

Future Recommendations:

From an examination of the results derived from this study, it must be concluded that the $0_3/H_20/0H$ interference problem can, in

TABLE I: COMPARISON OF REPRESENTATIVE FIELD MEASUREMENTS WITH LABORATORY OH INTERFERENCE EXPERIMENTS FOR THE CASE OF THE BOUNDARY LAYER

Field Study Location	Useable Laser Energy μJ	$[0_3]\times[H_20]$ (ppbv) × Torr	Raw Signal Photons/ 10 Min/Pmt	Ratio[a] Adjusted For Effects of Bandpass Filter and Geometry	Lab. Interf. Sig. / Tot. Field Sig.	Percent Interference
~16°N	162	3.7×10^2	1570	1884	.54	54
~ 3°S	126	4.3×10^2	2646	3175	.22	22
~ 8°S	165	4.2×10^2	2550	3060	.38	38
~14°S	190	3.8×10^2	2262	2714	.52	52
~25°S	152	3.1×10^2	2620	3144	.24	24
~38°N[b]	140	6.2×10^2	2256	2707	.48	48

(a) In the calculations of this ratio, the energy adjustment has been made relative to that quoted for the field study.

(b) This field data was collected during a 1976 field sampling program (not related to GAMETAG — Davis, et al., 1979) during which continental boundary-layer OH levels were measured — 0_3 levels were ~75 ppbv.

some cases, become serious if careful control is not maintained over the operational laser characteristics chosen in applying the LIF technique. Ideally, therefore, one would like to further reduce the restrictions that now must be placed on the LIF method and, at the same time, better quantify the magnitude of the 0H interference level under any and all field sampling conditions. In the first instance, consideration can be given to moving the laser pumping wavelength to the 306.0 nm (0,0) transition since both the quantum yield for $O(^1D)$ and the 0_3 absorption cross section would be lower there than at 281.9 nm. In this case, though, the weak fluorescence intensity of the (0,1) band at 342.8 nm results in an overall reduction in 0H detection sensitivity of at least a factor of ten relative to that derived from the 281.9 nm pumping scheme. Alternatively, the idea of both pumping and samping at the (0,0) band also appears impractical. If, for example, low resolution sampling optics were to be used the noise level from scattered 306 nm laser radiation would seriously reduce the OH detection sensitivity. On the other hand, high resolution sampling optics, which might eliminate the scattered 306.0 nm radiation problem, would result in an unacceptably poor optical sampling efficiency and thus again low 0H detection sensitivity. The latter shortcoming, though, would apply only to in-situ sampling of 0H and not necessarily to Lidar techniques.

A further expansion of the UV laser beam may also be considered as a tentative solution to the above 0H interference problem since the two-photon $0_3/H_20/0H$ interference scheme is obviously critically dependent on the laser energy density. With beam expansion, the interference problem could definitely be reduced, but very quickly the reduction in interference would be offset by a reduction in the efficiency of the collection optics for detecting natural 0H.

We believe that the best approach to further reducing the existing problem lies in the use of narrow laser pulses. The level of the 0H interference is seen from an adjacent paper (Tables I and II - Davis, et al., this issue GRL) to be critically dependent on the laser pulse width for times of 5 ns or less. For example, by reducing the nominal laser pulse width from 7 to .5 ns, and the $0_3/H_20/0H$ interference problem is reduced a factor of five or six (i.e., $0H_{Interf.}$ Signal/$0H_{Nat.}$ Signal). At this level, the 0H interference signal would be significantly less than the present random error in the LIF method (i.e., ~35%). No loss in sensitivity for detecting natural 0H would result from the use of narrow laser pulses. To this end, a modified laser system with a pulse width of .5 to 1.5 ns is presently under development in our lab.

A second modification proposed for future OH field measurement operations involves the quantification of the interference signal under field-sampling conditions. This is now possible with the availability of versatile tunable dye lasers and the availability of new information on the nascent 0H distribution resulting from the reaction of $O(^1D)$ with H_20. We have determined, for example, that for the $O(^1D) + H_20$ system, laser pumping of the $R_1(4)$, $R_1(5)$ transitions at 287.5 nm (corresponding to k = 4 and 5 in the v'' = 1 manifold of the $^2\Pi_{3/2}$state) produces a fluorescence intensity which is .82 of the fluorescence intensity derived from laser pumping the $Q_1(1)$ transition at 281.9 nm (Rodgers, et al., 1980). Thus, the possibility exists that during an 0H field sampling operation back-to-back measurements at 287.5 nm and 281.9 nm could quantatively establish the level of the 0H interference signal. In the latter sampling configuration, all signals derived from the $R_1(5)$, $R_1(4)$ transition would correspond to $0H_{Interf.}$; whereas, that from the $Q_1(1)$ transition could encompass both natural 0H and artificial 0H signal. This hypothesis will soon be tested in a new series of airborne measurements of 0H using a short pulse width laser system.

Conclusions:

Earlier estimates by us of the 0_3 $H_20/0H$ interference problem now appear to be too low. Based on a large volume of new information, we now have reassessed the magnitude of this problem for the case of the clean troposphere. We believe that the most reliable evaluation of the problem is that derived from the laboratory and field measurement studies employed. These studies indicate that for the GAMETAG 0H data collected in the tropical-marine boundary layer, the average midday interference correction, when compared to the total raw 0H signal, is 38%. For the tropical-marine free troposphere, the average midday interference level is estimated to be equal to or less than 15%. (Approximately 85% of all GAMETAG data were collected during the midday window of 10 AM-3 PM). Theoretical calculations suggest an interference level approximately a factor of 2 higher than the lab and field studies; but, considering the many possible sources of error in the calculations and to a somewhat lesser extent in the lab and field 0H measurements, we believe the agreement between theory and experiment to be quite good.

The absolute 0H interference signal predicted for subtropical and mid-latitudes will necessarily be much lower than that for the tropics since the H_20 level falls off much faster with latitude than does the increase in the 0_3 level. The percent interference, however, is not as easy to predict. As the H_20 level decreases with latitude, so will the natural 0H level. this decrease in natural 0H, due to the falloff in H_20, will be partially compensated by increases in the 0_3 level, but the natural 0H level will also decrease at high latitudes due to a reduction in the UV solar flux. In addition, the variability in the levels of C0 and N0 will cause significant variations in the natural 0H

level. Thus, exact quantitative calculations of the percent interference are difficult to carry out. A qualitative assessment of the latitudinal dependence of the 0H interference problem seems to suggest that during summer and spring months the percent interference should be somewhat lower at subtropical and mid-latitudes but perhaps somewhat higher at polar latitudes. The percent interference problem will certainly become far more severe during winter months at mid-latitudes. It is also quite evident that at all latitudes the percent interference will increase rapidly as the field sampling window is moved from midday to early morning or late afternoon.

One of the important findings of this work was that of identifying the laser pulse width as being the key laser parameter which could result in a major reduction in the $0_3/H_20/0H$ interference problem. Calculations show that a reduction in the pulse width from 7 to .5 ns could result in a factor of five to six reduction in the 0H interference level. Such a system is now under development.

ACKNOWLEDGEMENT

The author, D. D. Davis, would like to acknowledge the partial support of this research by the National Science Foundation (Grant #ATM-~~8007481~~ 7923598).

References

Chang, J.S., D.J. Wuebbles, and D.D. Davis, A Theoretical Model of Global Tropospheric 0H Distributions, UCRL Report #78392, February 1977.

Davis, D.D., M.O. Rodgers, S.D. Fischer, and W.S. Heaps, A Theoretical Assessment of the $0_3/H_20$ Interference Problem in the Detection of Natural Levels of 0H Via Laser Induced Fluorescence, this issue, GRL.

Rodgers, M.O., K. Asai, and D.D. Davis, OH Rotational Quantum State Distributions and Relaxation Efficiencies for the Reaction System: $0(^1D) + H_20 \rightarrow 2$ OH, Chem. Phys. Letters, in press, 1980.

Davis, D.D., W.S. Heaps, D. Philen, M. Rodgers, T. McGee, A. Nelson, and A.J. Moriarty, An Airborne Laser Induced Fluorescence System for Measuring OH and Other Trace Gases in the Parts-per-Quadrillion to Parts-per-trillion Range, Rev. Sci. Instr., 50, p. 1505, 1979.

Davis, D.D., M.O. Rodgers, D. Philen, and W.S. Heaps, "Erratum to above paper, Rev. Sci. Instr., in press, 1980a.

Davis, D.D., M.O. Rodgers, D. Philen, and W.S. Heaps, Tropical and Subtropical Boundary Layer 0H Measurements: A Test of Fast Photochemical Theory, submitted to J. Geo. Res., 1980b.

Davis, D.D., W. Heaps, D. Philen, and T. McGee, Boundary Layer Measurements of the OH Free Radical in the Vicinity of an Isolated Power Plant Plume: $S0_2$ and NO_2 Chemical Conversion Times, Atmos. Envir., 13, p. 1197, 1979.

(Received September 5, 1980;
accepted October 22, 1980.)

Attachment F

GEOPHYSICAL RESEARCH LETTERS, VOL. 8, NO. 1, PAGES 73-76, JANUARY 1981

A Theoretical Assessment of the O_3/H_2O Interference Problem in the Detection of Natural Levels of OH Via Laser Induced Fluorescence

D. D. Davis, M. O. Rodgers, and S. D. Fischer

School of Geophysical Sciences
Georgia Institute of Technology
Atlanta, GA 30332

and

W. S. Heaps

Goddard Space Flight Center
National Aeronautics and Space Administration
Greenbelt, MD 20771

Abstract. Theoretical calculations are presented which estimate the possible magnitude of the O_3/H_2O derived OH interference signal resulting from the use of the laser-induced fluorescence technique in measuring natural levels of tropospheric OH. Critical to this new assessment has been the measurement of the nascent OH quantum state distribution resulting from the reaction $O(^1D) + H_2O \rightarrow 2OH$, and an assessment of the subsequent rotational relaxation of the OH species when formed in high k levels.

Introduction

The OH radical has been indicated to be of critical importance to our understanding of tropospheric chemistry (Levy, 1971,74; McConnell, et al., 1971; Wofsy, et al., 1972; Crutzen, 1974; Davis, et al., 1979). To this end, the laser-induced fluorescence (LIF) technique has been developed with the objective of measuring atmospheric OH in the parts-per-quadrillion to parts-per-trillion concentration range (Davis, et al., 1979). The high sensitivity of the LIF method, however, can be compromised by the presence of an OH interference signal resulting from the laser photolysis of in-situ O_3, i.e.,

$$(1)\quad O_3 + h\upsilon(\lambda = 218.9\ nm) \longrightarrow O_2(^1\Delta) + O(^1D) \quad ,$$

followed by the very fast reaction (2),

$$(2)\quad O(^1D) + H_2O \longrightarrow OH + OH$$

or, alternatively, the deactiviation step (3)

$$(3)\quad O(^1D) + N_2\ (\text{or } O_2) \longrightarrow O(^3P) + N_2\dagger$$

To assess the magnitude of this OH interference signal, three approaches can be considered. First, a theoretical calculation of the artificially generated OH signal can be carried out based on available absorption cross section data, gas kinetic rate constants, a specified set of laser characteristics (i.e. energy, pulse width and beam diameter), and nominal atmospheric concentration levels of O_3, H_2O, N_2, and O_2. A second approach to this problem involves making direct measurements of the OH interference signal under laboratory conditions which simulate the real atmosphere and using laser parameters which closely parallel those employed under field-sampling conditions. The third and final approach can be defined as the most direct one and would involve an assessment of the OH interference signal based on actual field measurements of OH.

Reported in this paper is a theoretical assessment of the O_3/H_2O/OH interference problem. The calculations presented here have been made possible as a result of an independent study by these investigators (Rodgers, et al., 1980) in which the nascent OH quantum state distribution from rx. (2) and the subsequent rotational relaxation of the OH species via collisions with N_2, O_2, and/or H_2O have been measured.

Both laboratory and field measurement assessments of the O_3/H_2O/OH interference question are presented in an adjacent paper.

Results and Discussion

Theoretical Calculations:

From a consideration of reactions (1) through (3), the expression for the production of signal interfering OH radicals can be written as:

$$[OH]_{Interf.} = [O(^1D)]_{Total} \times \frac{2k_3[H_2O]}{k_3[H_2O] + k_2[N_2] + k_2'[O_2]} \qquad (A)$$

where those terms in square brackets are concentrations in molec./cm^3 and k_3, k_2, and k_2' are the gas kinetic rate constants for each respective reaction in units of cm^3/molec/s. The total $O(^1D)$ concentration can be calculated from the expression:

$$[O(^1D)]_{Total} = J_1[O_3]\tau_b \quad , \qquad (B)$$

where J_1 represents the photochemical rate constant for reaction (1) with units of s^{-1}, and τ_b is the base laser pulse width and thus encompasses the entire photon flux. For the case of weak absorption, true throughout the troposphere, J_1 can be further defined as:

$$J_1 = \frac{4I\,\sigma\,\phi}{\pi d^2} \qquad (C)$$

for the photolysis volume element $\frac{1}{4}\pi d^2\vartheta$, where d is the beam diameter and ϑ is the absorption path length (both in cm). σ and ϕ in equation (C) represent the absorption cross section and the quantum yield for production of $O(^1D)$ atoms at the photolysis wavelength of 281.9 nm. The laser intensity, I, can also be more usefully defined according to the equation:

$$\int_0^{\tau_b} I_0(t)dt = E/(\frac{hc}{\lambda}) \qquad (D)$$

Thus, equation (D) states that the intensity (photons/s) of the laser beam, when integrated over its total pulse width, τ_b, must yield the total number of photons in the beam. Substituting equation (D) into (C) then gives a final working expression for J_1 of:

$$J_1 = \frac{4E\sigma\phi\lambda}{\pi d^2 hc\tau_b} \qquad (E)$$

Returning now to equation (A), the OH interference concentration can be directly calculated if given a specific set of laser parameters, absorption cross section and quantum yield data, gas kinetic rate constants, and atmospheric concentrations of O_2, N_2, O_3, and H_2O:

Paper number 80L1579.
0094-8276/81/0080L-1579$01.00

$k_2 = 2.0 \times 10^{-11} Exp(107/T) cm^3/molec/s$ (Streit, et al. 1976)
E = 165 μJoules
$k_2' = 2.9 \times 10^{-11} Exp(67/T) cm^3/molec/s$ (Streit, et al. 1976)
λ = 281.9 nm
$k_3 = 2.0 \times 10^{-10} cm^3/molec/s$ (Wine & Ravishankara, 1980)
d = .85 cm (Davis, et al., 1980)
$\sigma = 3.3 \times 10^{-18} cm^3/molec$ (Inn & Tanaka, 1959)
$[N_2] = 1.9 \times 10^{19}$ molec/cm³
$\phi = 1.0$ (NASA Ref. Pub. 1010)
$[0_2] = 4.9 \times 10^{18}$ molec/cm³
$[H_20] = (18\ Torr) = 5.9 \times 10^{17}$ molec/cm³
$[0_3] = (20\ ppbv) = 5 \times 10^{11}$ molec/cm³
NOTE: τ_h divides out of equation (B).

The above atmospheric conditions are those typical of the tropical-marine boundary layer and are considered by us to be one of the worst situations for interference in the clean troposphere.

Based on the above input parameters, the calculated $[OH]_{Interf.}$ is given as $2 \times 10^8/cm^3$. Although this large artificial OH concentration would appear to totally dominate the estimated average midday (10 AM-3 PM) natural OH level of $1 \times 10^7/cm^3$, three important factors have yet to be considered. The first of these involves the fraction of the total $[OH]_{Interf.}$ that is present in a quantum state that can be excited with a 281.9 nm laser (i.e., $Q_1(1)$ electronic transition). In the case of natural OH, at 298 K (temperature of the tropical marine boundary layer) ~20% of the population is present in the $^2\pi_{3/2}$ k = 1 rotational state in the v'' = 0 manifold and is therefore excitable. Information on the fraction of $[OH]_{Interf.}$ in this same quantum state has heretofore been unavailable, as has the degree of rotational relaxation of OH radicals born in higher k levels during the nominal laser pulse width of 7ns. Both of these questions have now been addressed in our laboratory (Rodgers, et al. 1980), the final results showing that the average nascent population in the $^2\pi_{3/2}$ k = 1, v'' = 0 level could range from 4.5 to 2.9% of the total $[OH]_{Interf.}$ In addition, observations made under atmospheric conditions (i.e. 590 Torr N_2, 150 Torr 0_2, and 17 Torr H_20) showed that no appreciable rotational relaxation occurs during the laser pulse width of 7 ns. Some adjustment, however, must be made for a signal contribution from the k = 3 level in the v'' = 0 manifold of the $^2\pi_{1/2}$ state, the $R_2(3)$ transition from this state being coincident with the $Q_1(1)$ and $Q_1(1')$ transitions at 281.9 nm. The latter point will be addressed again later in the text. The upper value for the $^2\pi_{3/2}$ k = 1 population (i.e. 4.5%) is that defined by one of the OH radicals from rx. (2) being born with a rotational population distribution corresponding to 500 K in the v'' = 0 manifold, with the second OH radical being born in higher k levels of the v'' = 0 manifold as well as in the v'' = 1 and v'' = 2 manifolds (Rodgers, et al., 1980; Engleman, 1965). The lower population value of 2.9% would be the case if the first OH radical were spread out over the first 15 k levels of the v'' = 0 manifold; whereas, the second OH populated still higher k levels in the v'' = 0 manifold (k = 16-24) and also the v'' = 1 and v'' = 2 manifolds. (Rodgers, et al., 1980, have shown that k levels up to 24 are populated in the v'' = 0 manifold.) From the above population estimates it can readily be estimated that the excitable $[OH]_{Interf.}$ is reduced to a concentration which is only 2.9 to 4.4 times greater than the estimated midday $[OH]_{Nat.}$

The second factor which can influence the detectable signal from $[OH]_{Interf.}$ is related to the requirement that two photons are needed to produce an OH signal in the $0_3/H_20$ interference scheme. This means that OH produced in the second half of the laser pulse can not be detected by photons originating in the front portion of the laser pulse. Thus, the quantitative treatment of this problem requires a time-dependent model which takes into consideration the actual shape of the laser pulse. Further details on this point will be presented in a subsequent discussion.

The final factor that impacts on the efficiency with which $[OH]_{Interf.}$ is detected involves the time-dependence for the formation of OH from $O(^1D)$ atoms. Hanabusa, et al. (1977) have previously examined the effect of laser pulse width on the OH interference signal. These investigations, however, maintained constant laser power as the laser pulse width was varied. Their observed linear increase in the OH interference signal thus resulted from a continuous increase in laser energy. The latter experimental results are not relevant to the existing study where the OH interference signal needs to be measured as a function of laser pulse width at constant energy. In the ideal case, if the laser pulse were to be made very short compared to the $O(^1D)$ lifetime, virtually no OH interference signal would be detected since insignificant levels of OH would be formed during the laser pulse. For a 7 ns pulse, the fraction of the $O(^1D)$ reacting is fairly large but still requires the use of a time-dependent model calculation.

In the text that follows, we have presented two time-dependent models which are designed to show the detection efficiency of $[OH]_{Interf.}$ relative to $[OH]_{Nat.}$. In our case we have taken two examples for the laser pulse shape, a square wave and a sine wave. (Based on fast oscilloscope measurements, the actual laser pulse appears to be much closer to a square wave in its characteristics than to a sine wave.) The square and sine wave profiles lead to the following normalized laser intensities.

$$\text{Square Wave:} \quad I = E\lambda/hc\tau \tag{F}$$

$$\text{Sine Wave:} \quad I = E\lambda/hc \times \frac{\pi}{3\tau} \sin\left(\frac{2\pi}{3\tau} t\right) \tag{G}$$

In both cases, τ represents the full width of the laser pulse at half maximum intensity. Use of equations (F) and (G), in conjunction with equation (E), then allows one to define J_1 and the time-dependent production of $O(^1D)$, i.e.

$$\frac{d[O(^1D)]}{dt} = J_1[0_3] - [O(^1D)](k_3[H_20] + k_2[N_2] + k_2'[0_2]) \tag{H}$$

The time dependent OH concentration is then given by:

$$\frac{d[OH]_{Interf.}}{dt} = 2k_3[H_20][O(^1D)] \tag{I}$$

Solving both equations (H) and (I) for the case where $H_20 >> O(^1D)$ and the percent absorption of the laser beam by 0_3 is small, one can address the questions of the efficiency with which $OH_{Interf.}$ is excited to fluorescence relative to that of $OH_{Nat.}$. The magnitude of the $OH_{Interf.}$ fluorescence signal will be given by:

$$(OH_{Interf.})\ Fluor. \propto \int_0^{\tau_h} [OH]_{Interf.} \times (F_{Interf.})\ I(t)dt / \int_0^{\tau_h} I(t)dt \tag{J}$$

The proportionality constant in equation (J) is related to the efficiency of the detection optics and is thus the same for both $OH_{Interf.}$ and $OH_{Nat.}$. The ratio of the fluorescence signal from each OH type can then be expressed as:

$$\frac{(OH_{Interf.})Fluor.}{(OH_{Nat.})\ Fluor.} = \frac{\int_0^{\tau_h} [OH]_{Interf.} I(t)dt / \left(\frac{E\lambda}{hc}\right)}{[OH]_{Nat.}} \times \left(\frac{F_{Interf.}}{F_{Nat.}}\right) \tag{K}$$

Solving eq. (K) for both the square and sine wave pulse shapes yields:

SQUARE WAVE

$$\frac{(OH_{Interf.})Fluor.}{(OH_{Nat.})Fluor.} = \frac{\alpha}{[OH]_{Nat.}} \left[\frac{1}{2} - \frac{1}{\pi\chi}\left(1 + \frac{\exp(-\pi\chi)-1}{\pi\chi}\right)\right] \tag{L}$$

SINE WAVE

$$\frac{(OH_{Interf.})Fluor.}{(OH_{Nat.})Fluor.} = \frac{\alpha}{[OH]_{Nat.}} \left[\frac{1}{2} - \left(\frac{1}{(9\chi^2+4)}\right)\left(\frac{3\pi\chi}{4} + \frac{1 + \exp(-\frac{3}{2}\pi\chi)}{(\frac{9}{4}\chi^2+1)}\right)\right] \tag{M}$$

TABLE Ia: Theoretical Assessment of the 0H Interference Problem for the Case of the Tropical-Marine Boundary Layer[a]

LASER PULSE WIDTH, ns	.5				2				7				
Laser Energy μJoules	Sine (e) Ratio	Sine (b) % Interf.	Square (e) Ratio	Square (b) % Interf.	Sine (e) Ratio	Sine (b) % Interf.	Square (e) Ratio	Square (b) % Interf.	Sine (e) Ratio	Sine (b) % Interf.	Square (e) Ratio	Square (b) % Interf.	(c) % Interf. Corr. for $R_2 3$
100	.15	13	.16	14	.52	34	.48	32	.90	47	.87	47	51
(165)[d]	.29	22	.26	21	.86	46	.80	44	1.5	60	1.4	58	62
200	.35	26	.32	24	1.0	50	.96	49	1.8	64	1.7	63	67
300	.53	35	.47	32	1.6	62	1.5	60	2.7	73	2.6	72	76

(a) Interference calculations are based on one OH fragment from reaction (2) being born with a quantum state distribution which reflects a 500 K Boltzmann distribution (see Rodgers, et al. 1980)

(b) The percent interference is defined as $OH_{Interf.}$ Signal/Total OH Signal

(c) The correction for the signal derived from the $R_2 3$ transition has been made for $OH_{Interf.}$ species as well as $OH_{Nat.}$

(d) The "useable" laser energy which most typifies GAMETAG boundary-layer field measurements.

(e) Ratio = $OH_{Interf.}$ Signal/$OH_{Nat.}$ Signal, where $OH_{Nat.} = 1 \times 10^7/cm^3$.

TABLE Ib

Theoretical Assessment of the OH Interference Problem for the Case of the Tropical-Marine Boundary Layer [a]

LASER PULSE WIDTH, ns	7				
Laser Energy μJoules	Sine (e) Ratio	Sine (b) % Interf.	Square (e) Ratio	Square (b) % Interf.	(c) % Interf. Corr. for $R_2 3$
100	.60	38	.56	36	39
(165)[d]	.97	49	.93	48	51
200	1.2	55	1.1	52	55
300	1.8	64	1.7	63	67

(a) Interference calculations based on one 0H fragment from reaction (2) populating the first 15 k levels in the $v'' = 0$ manifold (as per Rodgers, et al. 1980)

(b) The percent interference is defined as $0H_{Interf.}$ Signal/Total 0H Signal.

(c) The correction for the signal derived from the $R_2 3$ transition has been made for $OH_{Interf.}$ species as well as $OH_{Nat.}$

(d) The "useable" laser energy which most typifies GAMETAG boundary-layer field measurements.

(e) Ratio = $OH_{Interf.}$ Signal/$OH_{Nat.}$ Signal, where $OH_{Nat.} = 1 \times 10^7/cm^3$

where:

$$\alpha = \frac{8k_3\phi\sigma E\lambda[0_3][H_20]}{\pi d^2 hcK} \times \frac{(F)_{Interf.}}{(F)_{Nat.}} \quad ,$$

$$\chi = \frac{K\tau}{\pi} \quad ,$$

$$K = k_3[H_20] + k_2[N_2] + k_2'[0_2] \quad ,$$

and $(F)_{Interf.}$ and $(F)_{Nat.}$ are the fractions of the interference 0H and natural 0H that are in the $^2\pi_{3/2}$, $k = 1$, $v'' = 0$ quantum state. From equations (L) and (M) it can be seen that the ratio of the interference 0H signal to the natural 0H signal is linearly dependent on the laser energy. The ratio of signals is also inversely proportional to the square of the laser beam diameter, reflecting the power density requirement of the two-photon interference scheme. Finally, it is seen that the interference signal increase relative to the natural 0H signal as the product $[0_3] \times [H_20]$ increases. Expressions (L) and (M), however, are somewhat misleading in that, for a given set of solar conditions, an increase in the product $[0_3] \times [H_20]$ would also likely increase the level of natural 0H. In general, though, the increase in the natural 0H level is likely to be somewhat less than that arising from the laser source.

TABLE II

Theoretical Assessment of the OH Interference Problem for the Case of the Tropical-Marine Free Troposphere[a]

LASER PULSE WIDTH, ns	7				
Laser Energy μJoules	Sine (e) Ratio	Sine (b) % Interf.	Square (e) Ratio	Square (b) % Interf.	(c) % Interf. Corr. for $R_2$3
100	.12	11	.11	10	12
200	.24	19	.23	19	21
(250)[d]	.30	23	.29	22	25
400	.48	33	.46	31	34

(a) Interference calculations based on one 0H fragment from reaction (2) populating the first 15 k levels in the $v'' = 0$ manifold (as per Rodgers, et al. 1980).

(b) The percent interference is defined as $0H_{Interf.}$ Signal/Total 0H Signal.

(c) The correction for the signal derived from the $R_2$3 transition has been made for $0H_{Interf.}$ species as well as $0H_{Nat.}$

(d) The "useable" laser energy which most typifies GAMETAG free-tropospheric field measurements.

(e) Ratio = $0H_{Interf.}$ Signal/$0H_{Nat.}$ Signal, where $0H_{Nat.} = 2.5 \times 10^6/cm^3$.

The interference ratios calculated from equations (L) and (M) have been summarized here in the form of Tables Ia, Ib, and II. Tables Ia and Ib represent the results for the tropical-marine boundary layer, using the earlier estimated 4.5% and 2.9% population values for $0H_{Interf.}$ in the k = 1 level. Table II is for the case of the tropical-marine free troposphere (excluding the ITCZ region), for the case of 2.9% of the total 0H population being in the $v' = 0$, k = 1 level. The average set of conditions taken for the tropical free troposphere (i.e., $[N_2]$ = 295 Torr, $[0_2]$ = 75 Torr, $[H_2O]$ = .6 Torr, and $[0_3]$ = 35 ppbv) reflect data recorded during the 1977/78 GAMETAG field-sampling program (Routhier, et al. 1980; Routhier and Davis, 1980).

In Tables I and II, both the signal ratio value and the percent interference have been given. In addition, each Table has a column which shows the effect of the R_2(3) quantum transition on the interference level. Finally, in Table I the dependence of the interference signal on the laser pulse width as well as laser energy is shown.

From Tables Ia and Ib it can be seen that for a laser energy of 165 μJ, in the tropical-marine boundary layer, the calculated interference is in the range of 51 to 62% (based on the square wave model). Table II, on the other hand, suggests a tropical free-tropospheric interference level of 25% for an energy of 250 μJ (34% if the k = 1 population is taken to be 4.5% rather than 2.9%). In each case, the laser energy cited represents the "useable" laser energy in the LIF system (Davis, et al., 1980) employed in the GAMETAG field studies. Approximately seventy-five percent of all GAMETAG 0H measurements were recorded at energies either equal to or less than the above levels.

The possible sources of error in these results are numerous and include: (1) the diameter of the laser beam (i.e., ~30% of the photons lie outside the .85 cm diameter quoted); (2) the reliability of the quantum yield for production of $O(^1D)$ atoms from 0_3 photolysis (a report by Lawrence and Stone, 1976 — private communication — has suggested that this value may be .87 instead of 1.0); (3) the accuracy of the gas kinetic rate constants employed for processes (2) and (3); (4) the uncertainty remaining in the nascent 0H population derived from reaction (2); and (5) possible uncertainties yet remaining in the time-dependent model for calculating the interference signal. At this point, even though the direction and magnitude of each of these errors is difficult to evaluate, the possibility of an overall uncertainty in these calculations of a factor of two seems likely.

A further analysis of the possible magnitude and direction of the error involved in the theoretical assessment of the $0_3/H_20/0H$ interference problem will be given in an adjacent paper by these same authors. In that paper, a comparison will be made between the theoretical predictions and experimental results based on laboratory and field measurements.

ACKNOWLEDGEMENT

The author, D. D. Davis, would like to acknowledge the partial support of this work by the National Science Foundation (Grant #ATM-8004781).
7923598

References

Crutzen, P.J., Photochemical Reactions Initiated by and Influencing Ozone in Unpolluted Tropospheric Air. Tellus, 26, pp. 47-57, 1974.

Davis, D.D., A.R. Ravishankara, and S. Fischer, SO_2 Oxidation via the Hydroxyl Radical: Atmospheric Fate of HSO, Radicals, Geo. Res. Letters, 6, p. 113, 1979.

Davis, D.D., W.S. Heaps, D. Philen, M. Rodgers, T. McGee, A. Nelson and A.J. Moriarty, An Airborne Laser Induced Fluorescence System for Measuring 0H and Other Trace Gases in the Parts-per-Quadrillion to Parts-per-Trillion Range, Rev. Sci. Instr., 50, p. 1505, 1979.

Davis, D.D., M.O. Rodgers, D. Philen, and W.S. Heaps, "Erratum" to above paper, Rev. Sci. Instr., In press, 1980.

Engleman, Jr., R., J.A.C.S., 87:18, p. 4193, 1965.

Hanabusa, M., C.C. Wang, S. Japar, D.K. Killinger and W. Fisher, Pulse-width Dependence of Ozone Interference in the Laser Fluorescence Measurement of 0H in the atmosphere, J. Chem. Phys., 66, p. 2118-2120, 1977.

Inn, E.C.Y. and Y. Tanaka, Ozone Absorption Coefficients in the Visible and Ultraviolet Regions, ADV Chemistry Series, Vol. 21, Amer. Chem. Soc., Wash., D.C., pp. 263-268, 1959.

Levy, H., Normal Atmosphere: Large Radical and Formaldehyde Concentrations Predicted, Science, 173, p. 141, 1971.

Levy, H., Photochemistry of the Troposphere, Advances in Photochemistry, 9, pp. 364-523, 1974.

McConnell, J.C., M.B. McElroy, and S.C. Wofsy, Natural Sources of Atmospheric CO, Nature, 233, p. 187, 1971.

NASA Reference Publication 1010, Robert D. Hudson, Editor, Chlorofluoromethanes and the Stratosphere, 1977.

Rodgers, M.O., K. Asai, and D.D. Davis, 0H Rotational Quantum State Distributions and Relaxation Efficiencies for the Reaction System: $O(^1D) + H_2O \rightarrow 2$ OH, Chem. Phys. Letters, In press.

Routhier, F.X., R. Dennett, A. Wartburg, P. Haagenson, A.C. Delany, and D.D. Davis, Free-Tropospheric and Boundary-Layer Airborne Measurements, of Ozone Over the Latitude Range of 58°S to 70°N, J. Geo. Res., 1980, In press.

Routhier, F.X. and D.D. Davis, Free-Tropospheric and Boundary-Layer Airborne Measurements of H_2O Over the Latitude Range of 58°S to 70°N: Comparison with O_3 and CO Data, J. Geo. Res., 1980, In press.

Streit, G.E., C. J. Howard, A.L. Schmeltekopf, J.A. Davidson and H.I. Schiff, Temperature Dependence of $O(^1D)$ Rate Constants for Reactions with O_2, N_2, CO_2, O_3, and H_2O, J. Chem. Phys., 65, p. 4761, 1976.

Wine, P. and A.R. Ravishankara, Deactivation of $O(^1D)$ by the Atmospheric Gases N_2, N_2O, H_2O, H_2, CO_2, and O_3, Chem. Phys. Letters, In press.

Wofsy, S.C., J.C. McConnell, and M.B. McElroy, Atmospheric CH_4, CO, and CO_2, J. Geo. Res., 77, p. 4477, 1972.

(Received September 5, 1980;
accepted November 22, 1980.)